



Probability distributions of land surface wind speeds over North America

Yanping He,¹ Adam Hugh Monahan,¹ Colin G. Jones,² Aiguo Dai,³ Sebastien Biner,⁴ Daniel Caya,⁴ and Katja Winger²

Received 2 July 2008; revised 21 September 2009; accepted 2 October 2009; published 18 February 2010.

[1] Knowledge of the probability distributions of surface wind speeds (SWS) is essential for surface flux estimation, wind power estimation, and wind risk assessments. The two-parameter Weibull distribution is the most widely used empirical distribution for SWS. This study considers the probability density function (PDF) of 3-hourly observations from 720 weather stations over North America for the period 1979–1999. The PDF of SWS is classified by season, time of day, and land surface type. The Weibull PDF is characterized by a particular relationship between the mean, standard deviation, and skewness. While the moments of the observed daytime SWS PDF are found to collapse around this Weibull relationship, the observed nighttime PDF has a broader range of values and is significantly more skewed than the Weibull PDF over rough surfaces. An idealized model shows that SWS skewness has a much greater rate of change with both the mean and standard deviation of surface buoyancy flux under conditions of stable stratification than that of unstable stratification. This result suggests that surface buoyancy flux plays an important role in generating diurnal variation of SWS PDF. Two global reanalyses products (ERA-40 and NCEP-NCAR) and three regional climate models (RCMs) (Rossby Centre Atmospheric Model version 3 (RCA3), limited area version of Global Environmental Multiscale Model (GEM-LAM), and Canadian Regional Climate Model, version 4 (CRCM4)) all have a less skewed nighttime PDF and a more narrow range of the normal wind speed during day and night. Among them, two of the RCMs capture the observed SWS differences across different land cover types, and only one of the RCMs produces the observed seasonal peak of SWS PDF.

Citation: He, Y., A. H. Monahan, C. G. Jones, A. Dai, S. Biner, D. Caya, and K. Winger (2010), Probability distributions of land surface wind speeds over North America, *J. Geophys. Res.*, 115, D04103, doi:10.1029/2008JD010708.

1. Introduction

[2] Surface winds are a fundamental meteorological variable, driven by pressure gradients, the Coriolis force, boundary layer mixing, and surface friction. Knowledge of the land surface wind probability density function (PDF) is important for many applications in wind energy resource assessment, extreme weather forecasting, and surface flux estimation [Petersen *et al.*, 1998a, 1998b; Jagger *et al.*, 2001; Monahan, 2006a]. In particular, the wind power density is proportional to the value of the third power of wind speed at heights of 20 to 80 m, which is coupled to surface winds and can be sufficiently determined by the first three moments of the probability distribution (mean, stan-

dard deviation, and skewness) of the PDF [Hennessey, 1977].

[3] A variety of parametric models have been proposed to describe surface wind speed (SWS) probability distributions in earlier studies. Among them, the two-parameter Weibull distribution has been suggested as a good empirical representation of the SWS PDF over land and sea [Hennessey, 1977; Justus *et al.*, 1978; Conradsen and Nielsen, 1984; Pavia and O'Brien, 1986]. For the Weibull distribution, the skewness is a unique function of the ratio of the mean to the standard deviation. Currently, this distribution is the most widely used PDF for applications in observational based wind power estimation over the globe [Elliott *et al.*, 1986; Justus *et al.*, 1976; Hennessey, 1977], wind risk assessment in the United Kingdom [Quine, 2000], hurricane wind intensity estimation in the United States [Jagger *et al.*, 2001], and downscaling of wind speed in northern Europe [Pryor *et al.*, 2005b]. It is the empirical distribution used for estimation of wind climate and annual wind energy production in WAsP, a commonly used tool for wind resource predictions on land (WAsP) (see Mortensen *et al.* [1993] and www.wasp.dk). However, previous studies have shown that the Weibull distribution does not provide an exact fit at

¹School of Earth and Ocean Science, University of Victoria, Victoria, British Columbia, Canada.

²Centre ESCER, University of Quebec at Montreal, Montreal, Quebec, Canada.

³National Center for Atmospheric Research, Boulder, Colorado, USA.

⁴Ouranos, Montreal, Quebec, Canada.

some land locations [Stewart and Essenwanger, 1978; Tuller and Brett, 1984] and generally over the oceans [Monahan, 2006a, 2006b]. Furthermore, as an empirical downscaling method, the success of the Weibull model relies on a strong and stationary relationship between predictors and predicted variables [Pryor et al., 2005b], and may misrepresent land SWS PDF under physical conditions when the relationship does not hold. Physically based stochastic models have been developed for the PDFs of variables such as sea surface temperature [e.g., Sura et al., 2006] and sea surface winds [e.g., Monahan, 2006a, 2006b], which provide an efficient and physically consistent tools for understanding and representing the PDF of a climate variable. Such mechanistically based PDFs bridge the gap between statistics and physics. A first step toward the development of a physical understanding of the origin of land SWS PDF is the characterization of the SWS PDF over different surface types and through the diurnal and annual cycles.

[4] The atmospheric boundary layer (ABL) is the layer of air directly above the surface in which the effects of the surface friction and surface heating and cooling are felt directly on time scales of less than one day. Over land in particular, the structure of the ABL is strongly influenced by the diurnal cycle of surface heating and cooling. Detailed terrain and surface roughness variations are fully considered in current wind atlas methodology; however, there is not at present a physical understanding of the relationship between surface buoyancy fluxes and the SWS PDF [Landberg et al., 2003]. To fully characterize the SWS distribution, this study investigates the dependence of SWS PDF on land cover type, season, and time of day (day versus night). This analysis uses data from surface stations, which measure the speed of air movement usually (but not always) about 10 m above the ground.

[5] In contrast to traditional wind atlas methods, regional climate models (RCMs) offer one means to consistently downscale large-scale climate information provided by coupled General Circulation Models (GCMs) to produce high-resolution, localized climate data consistent with the large-scale climate simulated by the GCM for present or future climates. As a result of their relatively high resolution (presently around 0.5° , with plans in many centers to increase this to $\sim 0.1^\circ$ in the near future), RCMs can provide increased detail for many GCM-simulated near-surface climate variables, particularly those influenced by local topography and surface type [Frey-Buness et al., 1995]. RCMs have been used in many applications such as the future wind potential change in the United States [Segal et al., 2001], the impact of potential climate change on wind energy resources in northern Europe [Pryor et al., 2005a], estimation of extreme SWS and its future changes over Europe [Rockel and Woth, 2007], and verification of the empirical downscaling of SWS over northern Europe [Pryor et al., 2005b]. Global reanalyses also provide surface wind products for wind climate estimation. In both reanalysis products and RCMs, the 10 m wind speed is vertically extrapolated from the bottom-level winds. In principle, the influence on surface winds of surface buoyancy fluxes has been included in the reanalysis and RCM turbulence mixing schemes and vertical extrapolation formulae. Given the importance of RCM simulations in predicting future changes in SWS variability and the utility of reanalysis

products as representations of long-term global-scale atmospheric variability it is useful to determine how well these modeled SWS distributions correspond to observations.

[6] The general objectives of this study are as following:

[7] 1. Identify those conditions in which the two-parameter Weibull distribution is a good fit to observations and those conditions in which it is not. This is done by characterizing the observed SWS PDF by season, time of day (day versus night) and land surface type.

[8] 2. Investigate how the dependence of surface drag on surface buoyancy flux influences the observed non-Weibull behavior of land surface winds at night. This is done using a simple stochastic model to study the relationship between leading three moments of SWS and surface buoyancy flux.

[9] 3. Evaluate current reanalysis and RCMs surface wind products and identify their ability to represent the observed characteristics of the SWS PDF. This is done both to evaluate the basic simulated statistics and to ascertain whether the observed sensitivity of the wind speed PDFs to factors such as diurnal and seasonal variations over different underlying land surface are faithfully represented in the models. The latter analysis will determine confidence in current RCM projections of any future changes in SWS PDFs and associated wind energy potential.

[10] The data and analysis methods are described in section 2; observational results and data set intercomparison are presented in section 3; the role of surface buoyancy on nighttime SWS PDF is addressed through a simple stochastic surface wind model study in section 4. A summary and conclusions are presented in section 5.

2. Data, Models, and Methods

2.1. Observational Data

[11] Three-hourly synoptic weather reports transmitted through the Global Telecommunication System (GTS) and archived at the National Center for Atmospheric Research (NCAR) are used here to characterize SWS PDF. This data set was described by Dai and Deser [1999]. It contains 3-hourly, 10 min averaged data of SWS usually (but not always) measured at around 10 m height at weather stations and reported in units of knots (1 knot = 0.514 m/s). Here we used the wind data from 1 January 1979 to 31 December 1999 over North America (0° – 70°N , 50°W – 160°W). Since May 1997, many North American stations contain hourly reports. For these cases, only the reports near the 3-hourly reporting times were selected and used in this study in order to maintain consistency with earlier records. An individual weather station is identified by its longitude and latitude (within 0.01°) and by its height (within 1 m). There are over one thousand stations in North America; from these we selected those stations that had at least 12 years with a total of 365×4 or more records each year. Of these stations, 719 have both sufficient wind records for both day and night; while one station at (105.13°W , 69.10°N) in northern Canada have enough wind records only for the nighttime.

[12] It should be pointed that there are some potential quality issues associated with this data set. First, as noted by Dai and Deser [1999], some of the wind records may have been taken at measurement heights other than the WMO-recommended 10 m above the ground. Unfortunately, the anemometer height is not included in the metadata of this

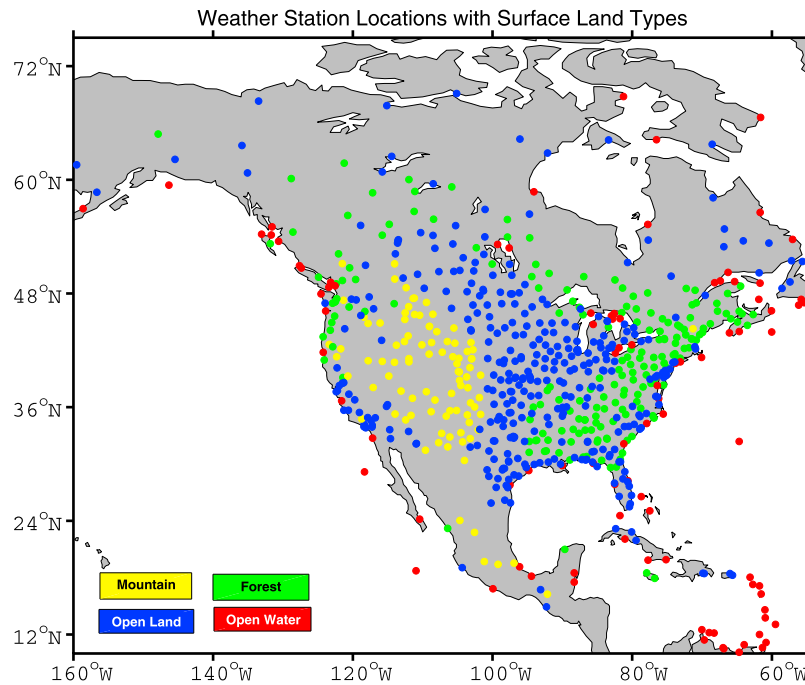


Figure 1. Spatial distribution of four land surface types (mountain ($z \geq 1000$ m), yellow; forest, green; open land, blue; and open water, red) for 720 North American weather stations.

data set. While variations in measurement height can affect the mean and std. of wind speed, we do not expect the shape of the PDF (the focus of this study) to vary greatly around that at 10 m as long as the measurements are taken at a fixed height. However, a small number of stations may have changed their measurement heights or the local environments may have changed (e.g., growth of trees or construction of new buildings nearby) during the data period (1979–1999). These changes could induce spurious changes in SWS records that could affect the PDFs and thus our results, although such changes often occur over much longer periods (e.g., 50–100 years) in climate records and are not expected to introduce a systematic error across observing locations. Unfortunately, it is difficult, if not impossible, to remove those spurious changes without detailed metadata. As the primary focus of this analysis is on the structure of the SWS PDF, following *Dai and Deser* [1999], we used the data without height adjustments in our analysis and verified the robustness of our results using different subsets of the data set (see below). Furthermore, any North American station records likely contain discontinuities resulting from a switch from conventional observing systems to automated observing systems around the mid-1990s [*National Weather Service*, 1992; *Doesken et al.*, 2002; *Dai et al.*, 2006], although wind measurements have always been made by anemometers. We have computed the first three moments of SWS and the North American regional SWS PDF for the periods of 1979–1993, 1994–1999, and 1979–1999 separately, and found that our main conclusions are the same for each of the periods. Thus, any discontinuities introduced by this change in observing systems appear to have little effect on our results. These tests also suggest that our results are robust over different data periods and are not very sensitive to potential discontinuities associated with observational and local environmental changes.

[13] The SWS PDFs will be classified by their first three moments (mean, standard deviation, skewness). The first two of these moments are measures of wind speed magnitude (of the average and the variability); in contrast, the skewness is interesting on its own as a measure of the shape of the SWS distribution. These moments are calculated for each season (December–February or DJF; March–May or MAM; June–August or JJA; and September–November or SON) using all years of the 1979–1999 data, and for day (from local sunrise to local sunset), and night (from local sunset to local sunrise). Sunset and sunrise times are calculated using NOAA Sunrise/sunset and solar position calculators, which are based on the astronomical algorithm of *Meeus* [1998]. For each station, there are up to 7665 wind records for each data subset (time of day, season) during the study period. As a result, we expect the leading three statistical moments to be reliably estimated. A preliminary analysis of the observations indicated the presence of a small number of strikingly large SWS values; in some but not all cases other simultaneous measurements were consistent with extreme weather. Because the goal of the present study is to characterize the probability distribution of surface wind speeds in standard conditions, the top 0.5% of station wind records was removed before calculating leading moments. The reasons for this removal and its effects of removing these extreme wind records on three leading moments are further discussed in Appendix A.

[14] The surface wind observations are also stratified according to surface type. A given weather station with an elevation greater than 1000 m is classified as mountain type; the remaining weather stations are classified as forest, open land, and open water, as derived from the collocated point within the ECOCLIMAP surface physiographic data set [*Masson et al.*, 2003]. The distribution of these four surface types over the study domain (Figure 1) shows that the open

Table 1. Number of Stations in the Four Land Cover Types From Observations, ERA-40 Reanalysis, NCAR NCEP Reanalysis, RCA3, GEM-LAM, and CRCM4 Regional Climate Models

	Mountain	Forest	Open Land	Open Water	Total
	<i>Day</i>				
Observation	93	189	343	94	719
ERA-40	93	189	343	94	719
NCEP	93	189	343	94	719
RCA3	93	189	343	94	719
GEM-LAM	93	187	314	67	661
CRCM4	88	186	335	69	678
	<i>Night</i>				
Observation	93	189	344	94	720
ERA-40	93	189	344	94	720
NCEP	93	189	344	94	720
RCA3	93	189	344	94	720
GEM-LAM	93	187	316	67	663
CRCM4	88	186	338	69	681

water-dominated stations are located in the coastal and large lake regions while a large fraction of forest-dominated stations are found in the eastern part of the United States and Canada. Most of open land-dominated stations are in the Great Plains of central North America, while the majority of mountain-dominated stations are in the western Cordillera.

2.2. Reanalyses and Regional Climate Models

[15] Along with observed surface winds, this study will consider the SWS PDF from reanalysis products and RCM simulations. Reanalysis products provide long-term characterizations of atmospheric fields, but at coarse spatial resolution and sensitive to the parameterizations of the reanalysis model. Monahan [2006b] demonstrated that the essential features of the SWS PDF over the global ocean were reasonably well captured (relative to scatterometer observations) by both the ERA-40 and NCEP-NCAR reanalyses. SWS from both the ERA-40 [Uppala *et al.*, 2005] (http://data-portal.ecmwf.int/data/d/era40_daily) and NCEP-NCAR [Kalnay *et al.*, 1996] (<http://www.cdc.noaa.gov>) reanalyses are instantaneous 6-hourly, 10 m winds at the two respective Gaussian grids, which we linearly interpolated onto $2.5^\circ \times 2.5^\circ$ latitude-longitude resolution for the study period (1979–1999). The wind fields from the following three regional climate models (RCM) are evaluated in this study: (1) the limited area version of GEM (Global Environmental Multiscale Model [Cote *et al.*, 1998; Zadra *et al.*, 2008], hereafter referred to as GEM-LAM), which is planned as the next Canadian Regional Climate Model; (2) the present Canadian Regional Climate Model, version 4 [Caya and Laprise, 1999; Plummer *et al.*, 2006; De Elia *et al.*, 2007] (hereafter CRCM4); and (3) The Rossby Centre Atmospheric Model version 3 [Jones *et al.*, 2004; Kjellström *et al.*, 2005] (hereafter RCA3). Each of the RCMs provides 3-hourly simulated 10 m wind fields at a horizontal resolution at $0.5^\circ \times 0.5^\circ$. The three RCMs were forced by analyzed lateral boundary conditions and observed sea surface temperatures (SSTs) and sea ice concentrations (SICs) for the period 1979–1999. Boundary conditions for the RCA3 and GEM-LAM simulations were derived from the ERA-40 reanalysis, while boundary con-

ditions for the CRCM4 simulations were derived from the NCAR NCEP reanalysis.

[16] For most RCMs and reanalyses, a grid point value represents the area mean of the whole grid box, which is indexed to the center of its grid box. For the purpose of this study, each RCM domain is divided into four land cover types (mountain, forest, open land and open water); to ensure that the observational, reanalysis, and RCM simulated SWS over different land types are directly comparable, only data from those reanalysis and RCM grid boxes near to stations in the observational record were considered. In particular, output at a given grid point is included in the analysis if (1) it has the same dominant land cover type as the nearest station; (2) its center lies within 100 km of the station; and (3) it is the closest of all the neighboring grid boxes. The above selection criteria are based on the assumption that surface wind climatology at a weather station is a good representation of the wind climatology of its neighboring small area with the same land surface type. Note that individual models divide the low-elevation ($z < 1000$ m) part of the grid domain into multiple land cover types: RCA3 has three land cover types (forest, open land, and open water); GEM has 26 land cover types, and CRCM4 has 5 types. In this study, we regroup GEM and CRCM4 land types into the three basic land cover types of RCA3, as determined by the ECOCLIMAP surface type. The dominant land cover type for a low-elevation RCM grid box is defined as the type that has the largest cover fraction. The surface types at weather stations and for ERA-40 and NCEP-NCAR reanalysis grid boxes over low-elevation regions are also determined by the ECOCLIMAP surface type. The numbers of stations for each land type for each data set are listed in Table 1.

3. Observed and RCM Simulated Land Surface Wind Speed PDF

3.1. Observed PDF

[17] The observational data set is used to compute the leading three moments (mean, standard deviation, and skewness) of SWS. Both the mean and standard deviations of SWS (hereafter $\text{mean}(w)$) and $\text{std}(w)$, with w denoting SWS) are significantly influenced by the underlying land surface (not shown). Generally speaking, the mean and its standard deviation of SWS are smaller over rougher surfaces and larger over smoother surfaces. Highest mean wind speeds are seen over smoother surfaces such as open water-dominated east and west coasts of Canada and the open land-dominated central belt of the United States; the smallest mean and standard deviation of SWS are found over rough surfaces such as forested areas in the eastern part of the United States and mountain-dominated regions in the western part of the Rocky Mountains (due to surface heterogeneity). These familiar features are consistent with previous studies of surface wind climatology and wind energy atlases, and are therefore not shown [Elliott *et al.*, 1986; Archer and Jacobson, 2003, 2005] (also WASP [Mortensen *et al.* [1993] and www.wasp.dk] and Canada Wind Atlas (www.windatlas.ca)).

[18] SWS skewness (hereafter $\text{skew}(w)$) represents the asymmetry of the PDF around its mean value, taking positive (negative) values if the PDF is tilted toward

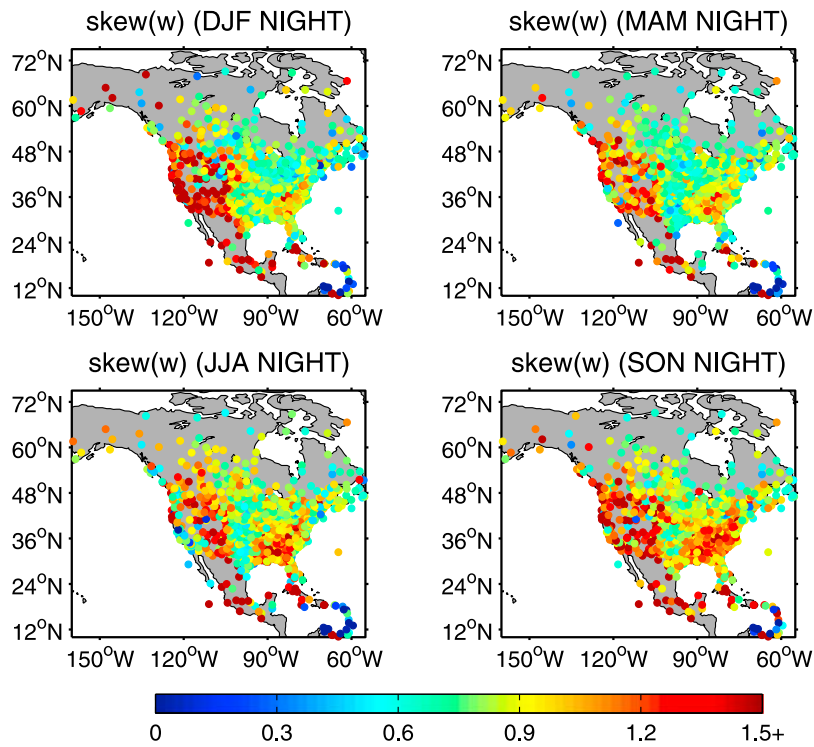


Figure 2. The observed nighttime skewness of surface wind speed during four seasons over North American weather stations during 1979–1999.

positive (negative) anomalies. The spatial distribution of both the observed nighttime skewness of surface wind speed (hereafter $skew(w)$) and the normalized wind speed (defined as the ratio $mean(w)/std(w)$) are shown in Figure 2 and

Figure 3, respectively, for four seasons over North America. Surface wind speeds are positively skewed at most stations; that is, the SWS PDF is characterized by tails toward large wind speeds. Note that although w is a nonnegative quan-

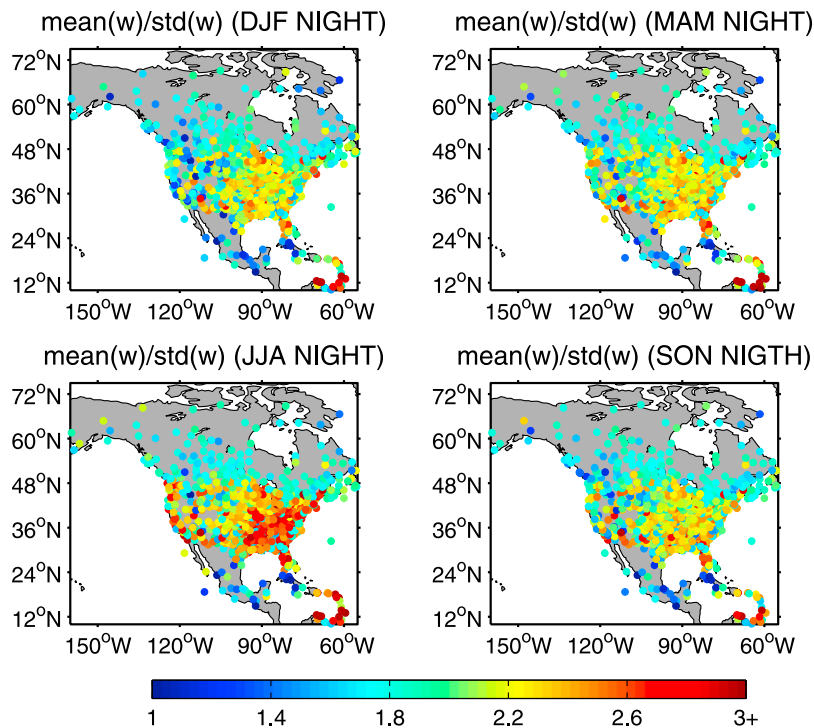


Figure 3. The observed nighttime normalized surface wind speed mean $mean(w)/std(w)$ during four seasons over North American weather stations during 1979–1999.

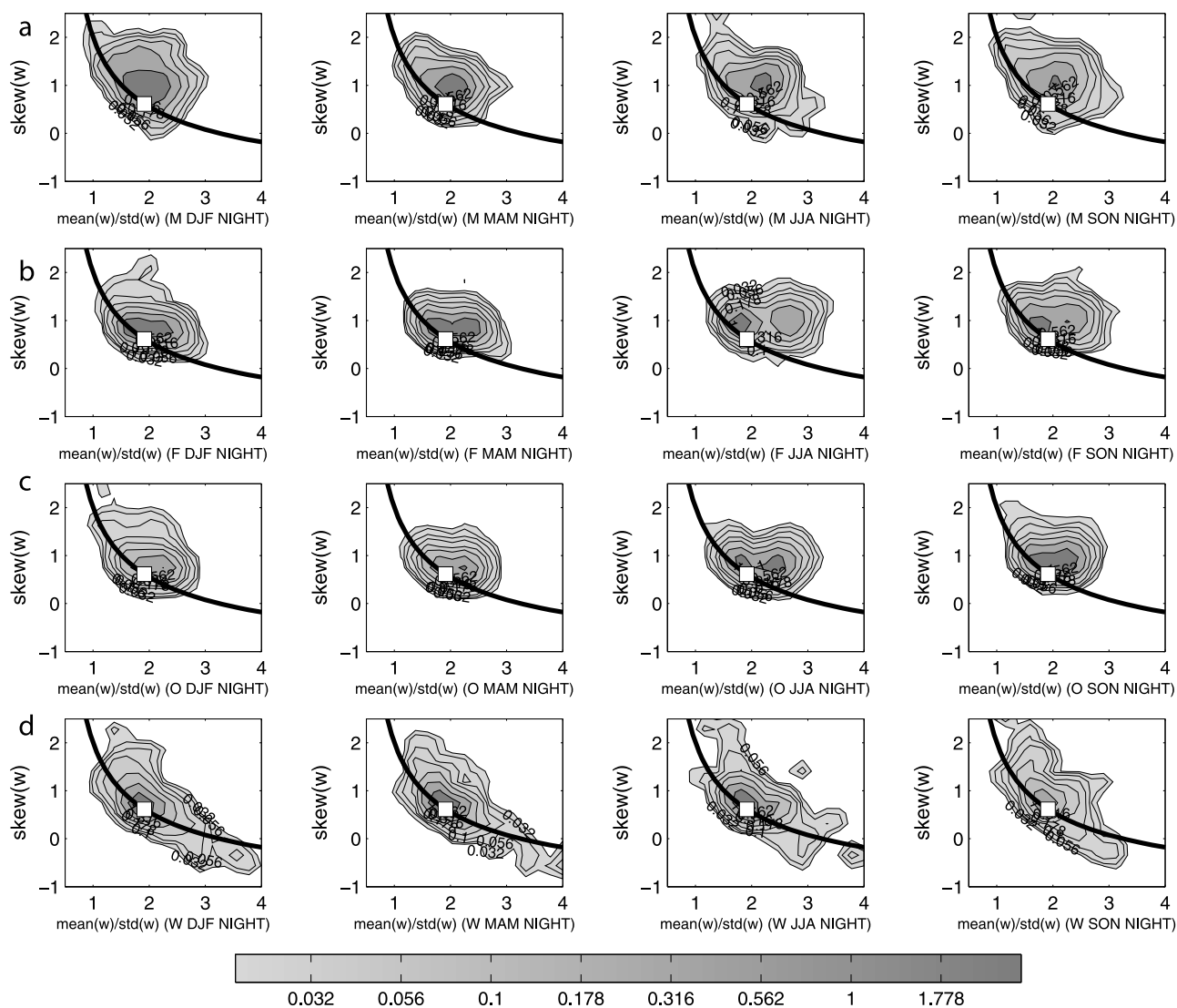


Figure 4. Kernel density estimates of joint pdfs of $\text{mean}(w)/\text{std}(w)$ and $\text{skew}(w)$ for nighttime weather station data over (a) mountain, (b) forest, (c) open land, and (d) open water regions in four seasons during 1979–1999. The contour intervals are logarithmically spaced. The solid line is the theoretical curve for a Weibull variable, and the white square corresponds to a Rayleigh variable (a special case of the Weibull distribution arising when the vector wind components are Gaussian, isotropic, and uncorrelated with mean zero).

tity, it is possible for the SWS PDF to be negatively skewed (as it is over much of tropical oceans [Monahan, 2006a]). Generally speaking, $\text{skew}(w)$ is larger over mountain regions such as the Rocky Mountains in the western United States and the Appalachian Mountains in the eastern United States than over the flat areas such as the central and eastern parts of the United States. Over low-elevation regions, $\text{skew}(w)$ has the smallest value over open water-dominated areas such as coasts and subtropical islands, and the largest values over forest-dominated regions such as the eastern United State and Canada.

[19] The two-parameter Weibull distribution is the most widely used empirical SWS probability distribution. For example, the WASP methodology for generating wind power atlases (WASP (Mortensen *et al.* [1993] and www.wasp.dk)) uses local information (surface roughness, terrain height, sheltering obstacles) along with regional

climate data to predict the Weibull parameters of the SWS PDF at a given location. A particular feature of the Weibull distribution is that $\text{skew}(w)$ is a unique function of the normalized wind speed such that the skewness is positive for small values of this ratio (weak, high-variability winds) and decreases monotonically to become negative for large values of the ratio (strong, low-variability winds) [Monahan, 2006a]. Estimates of the joint distribution of SWS skewness and normalized mean wind speed over the different surface types are presented in Figures 4 and 5 for nighttime and daytime, respectively, along with the corresponding curve for a Weibull distributed random variable. At night, the Weibull distribution substantially underestimates the skewness of SWS over mountains, forests, and open land for larger values of the normalized mean wind speed. In other words, it significantly underestimates the probability of relatively strong wind speeds during the night in rough

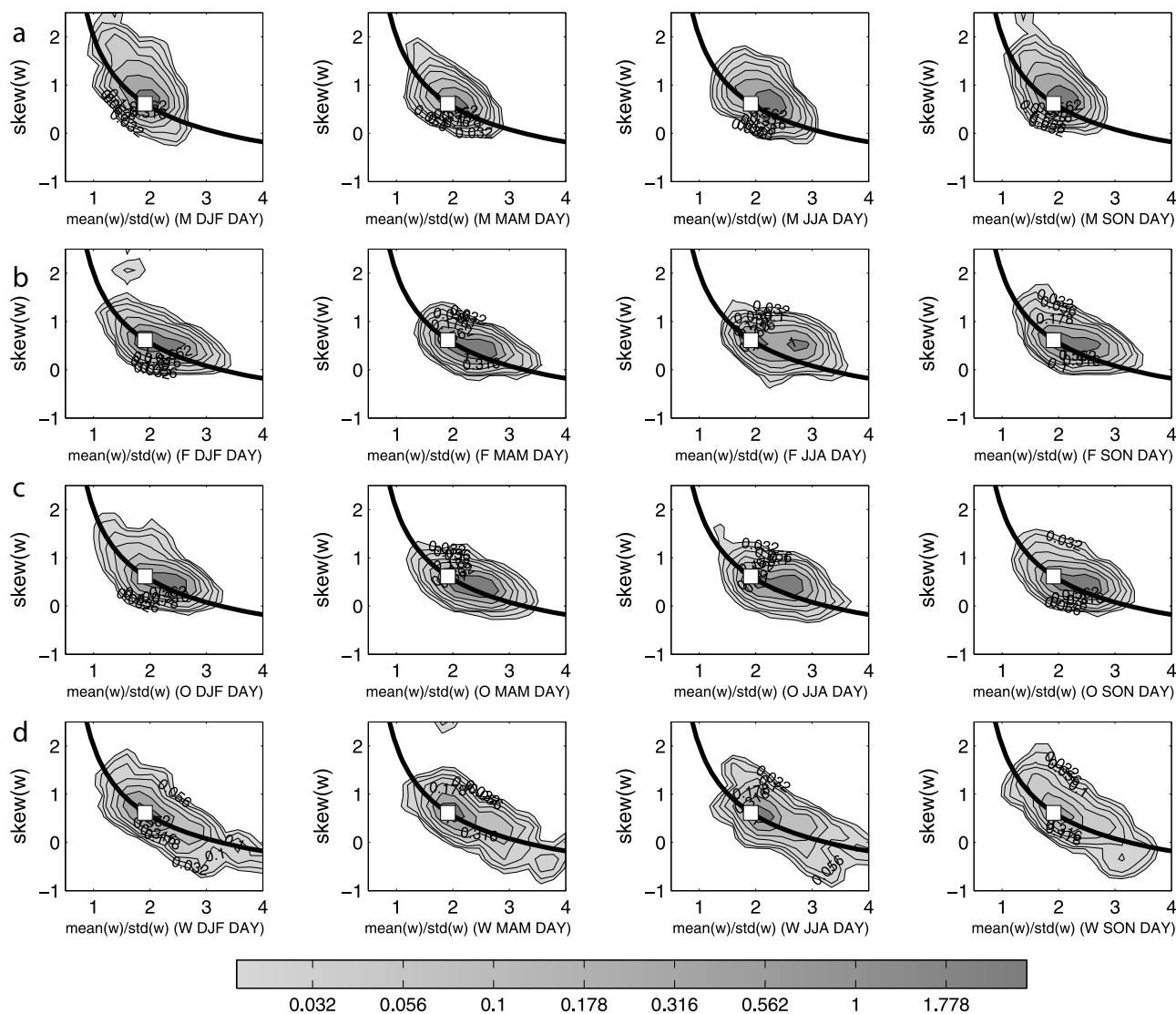


Figure 5. As in Figure 4 but for the daytime case.

locations characterized by typically strong and sustained winds. In contrast, for daytime winds, all the joint distributions cluster around the Weibull curve, demonstrating that in broad terms on a North American domain scale the Weibull distribution is a reasonable first-order model for daytime SWS PDF over all surface types and in all seasons (of course, some individual locations may show distinctly non-Weibull behavior).

[20] The spatial and seasonal structure of the diurnal variation in skewness is illustrated in Figure 6. It is evident that the diurnal variation in skewness is strongest in summer-autumn and weakest in winter-spring. In both JJA and SON seasons, nighttime skewness exceeds daytime skewness at more than 90% of the stations. The presence of a diurnal cycle in the shape of the SWS PDF, and the modulation of this diurnal cycle by the annual cycle, is suggestive of the influence of surface buoyancy fluxes. In fact, surface buoyancy fluxes are well known to drive a diurnal cycle in both the mean and standard deviation of SWS (modulated by both mesoscale and synoptic scale variability). These results indicate that not only the strength of the wind (and its

variability) change across the day, but also the shape of the SWS distribution. The influence of surface fluxes on the SWS PDF is discussed in greater details in section 4.

[21] It is worth noting that weather stations measure SWS in open air with no trees upwind to distances of 100 times the anemometer height and therefore the SWS may not be representative of winds directly over the forest canopy itself. Measurements from tall towers representing winds over the forest canopy are available from the AmeriFlux sites [Linacre, 1992]. We derived diurnal SWS PDF variations above the canopy using AmeriFlux Level 2 hourly wind speed data (unfilled) from 13 selected forest sites that have at least 3 years of data over North America. The name, locations, time period, and canopy height of these sites are listed in Table 2 (see also <http://public.ornl.gov/ameriflux> for more detailed description and site data). Figure 7 shows the observed relationship between skewness and its normalized wind speed during day and nighttime, along with the theoretical curve for a Weibull variable. The AmeriFlux results are consistent with our key finding from the weather station observations that the daytime SWS PDF collapses

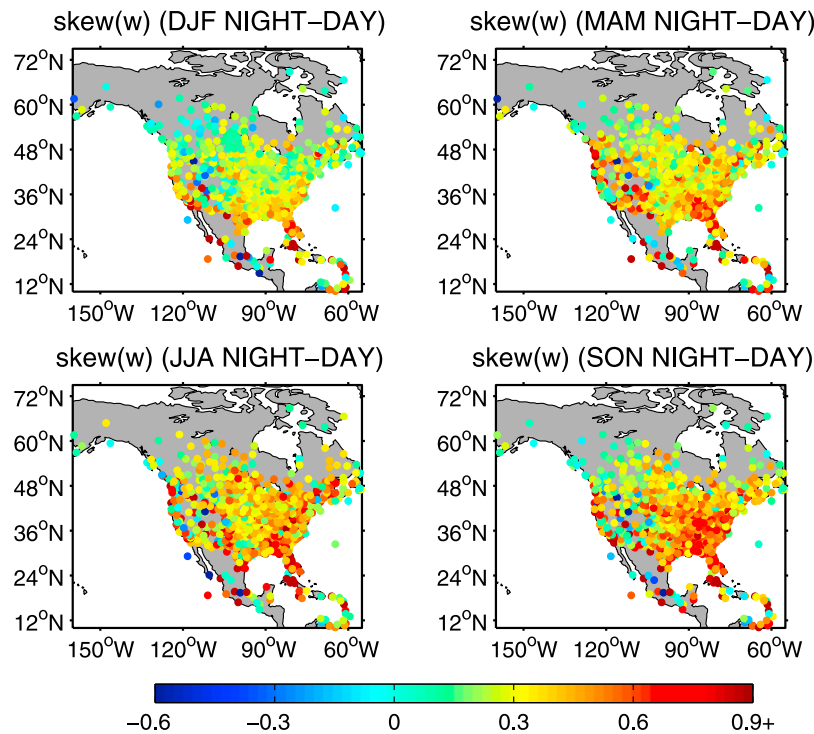


Figure 6. The skewness difference (nighttime minus daytime) of the observed surface wind speed during four seasons over North American weather stations during 1979–1999.

reasonably well around the Weibull distribution, but the nighttime SWS PDF is typically more positively skewed.

3.2. Reanalysis and RCM Simulations

[22] Standard current SWS PDF estimation tools make use assumptions regarding the parametric form of the PDF (e.g., Weibull) or assume neutral surface stratification [e.g., Landberg *et al.* 2003] (also Canada Wind Atlas). In contrast to statistical/empirical methods widely used in current SWS PDF estimation, global reanalysis models and RCMs offer consistent wind products directly influenced by surface buoyancy fluxes and local land surface types. In principle, these products allow for the investigation of variability of the SWS PDF on large spatial scales and long time scales, as well as in future climates. Of course, their utility for these purposes is contingent on their ability to accurately simulate

the observed features of SWS PDF, in particular, the dependence on surface type, season, and time of day.

[23] Averages over the North American domain of the nighttime SWS PDF (hereafter $NAP(w)$) histogram from observations, reanalysis products, and RCM simulations for each of the four land surface types are illustrated in Figure 8 for each of the four seasons. The sensitivity of the observed $NAP(w)$ to the underlying surface is clearly illustrated in Figure 8. All $NAP(w)$ peak at small wind speeds and long tails toward large wind speeds (i.e., are positively skewed). In all seasons, the nighttime tail toward large wind speed values is more pronounced over mountainous, open land– and forest-dominated surfaces than over open water. Of the reanalysis products and RCM simulations, only GEM-LAM and RCA3 represent the observed $NAP(w)$ difference over the four different land cover types; although GEM-LAM overestimates the vari-

Table 2. List of 13 AmeriFlux Forest Sites With Name, Location, Time Period, and Canopy Height

Name	Location	Time Period	Canopy Height
Willow Creek	(45.8059261, -90.0798592)	1998–2006	24.3 m
Walker Branch	(35.9587667, -84.2874333)	1995–2005	25 m
UMBS	(45.5598400, -84.7138200)	1999–2006	20 m
Morgan Monroe	(39.3231500, -86.4131390)	1999–2006	27 m
Missouri Ozark	(38.7441000, -92.2000090)	2004–2007	24.2 m
Metolius (old age)	(44.4991662, -121.5571658)	1996–2000	10–34 m
Metolius (intermediate age)	(44.4524325, -121.5571658)	2002–2007	14.0 m
Metolius (first young age)	(44.4371895, -121.5667560)	1999–2002	0.9–4.3 m
Howland forest (main tower)	(45.2040700, -68.7402778)	1996–2004	20 m
Flagstaff-unmanaged forest	(35.0897306, -111.7624972)	2005–2007	18 m
Flagstaff-managed forest	(35.1333333, -111.7275111)	2005–2007	18 m
Slashpine-Ponaldson-mid-rot	(29.7547667, -82.1632833)	1999–2005	13 m
Black Hill	(44.158, -103.650)	2001–2007	Conifer (~24 m)

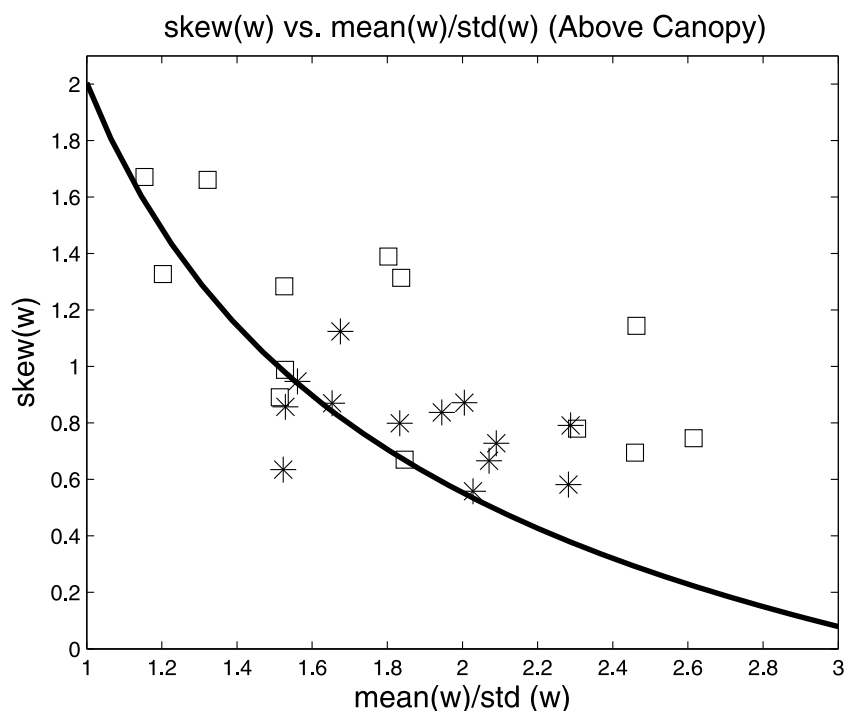


Figure 7. The observed relationship between skewness and normalized mean wind from AmeriFlux Level 2 data over 13 forest sites during daytime (asterisks) and nighttime (squares). The solid line is the theoretical curve for a Weibull variable.

ance of wind speeds over open land. Each of ERA-40, NCEP, and CRCM4 show little sensitivity to the underlying surface type in all seasons. Furthermore, the median wind speeds in ERA-40, NCEP NCAR, and RCA3 are underestimated and the tail of the distribution is overestimated in GEM-LAM and underestimated in RCA3 for open water-dominated regions. Figure 8 also shows that only RCA3 produces the observed seasonal maximum $NAP(w)$ peak at small wind speeds in JJA.

[24] Comparisons of daytime and nighttime standardized $NAP(w)$ (defined as the anomaly probability distribution of the North American domain wind speed $w' = \frac{w - (\text{domain_mean})}{(\text{domain_std})}$) histogram over all land surface types in SON are presented in Figure 9 for winds from observations, reanalysis products, and each of the RCMs. The observations display a strong day-night difference in standardized $NAP(w)$ over mountain- and forest-dominated surfaces, and a weak difference over open land- and open water-dominated surface. The observed SWS has a nighttime PDF that is more skewed than the daytime PDF over both mountain and forest regions; the two reanalysis products and three RCMs display either no diurnal cycle or substantially less skewed nighttime PDF over these two surface types. It is worth noting that in both reanalysis and RCMs, SWS is vertically extrapolated from their lowest bottom level winds. Problems related to the empirical extrapolation formula may account for the inadequate representation of diurnal extremes over North America. The failure to represent the day-night difference may also come from a general failure to capture the change in atmospheric turbulence during nighttime and the inability of most models to properly simulate the nocturnal boundary layer and in particular

changes in momentum transport (vertically in the lower atmosphere and as an exchange with the surface) under stable conditions.

[25] Estimates of the joint distributions of normalized wind speed and wind skewness from two reanalyses (ERA-40 and NCEP NCAR), and three RCMs (RCA3, GEM-LAM, and CRCM4) and all four seasons over the period 1979–199 are presented along with the Weibull distribution for daytime and nighttime in Figures 10 and 11, respectively. The RCM and reanalysis surface winds tend to cluster around the curve characteristic of the Weibull distribution in both day and night. Neither the reanalysis products nor the RCM simulations capture the observed nighttime non-Weibull behavior. The ERA-40 reanalysis shows a hint of the increased nighttime skewness in DJF, MAM, and SON seasons; while for the NCEP-NCAR reanalysis the JJA nighttime skewness is slightly greater than that of the daytime. This diurnal cycle is not present in any of the RCM simulations. Because two reanalyses use similar approaches as the three RCMs to parameterize surface momentum fluxes and near surface winds, their greater variability may arise from observational input through the assimilation process, which allows a larger variability of weather variables and systems than seen in the three RCMs.

[26] Particular caution is required when comparing station observations with simulated, grid-averaged surface winds over forested regions. Weather stations in forested areas are typically located in open clearings near or within forest areas. The land area in a RCM grid box is often classified into subdomains based on different land surface types; surface wind speeds are calculated separately for each

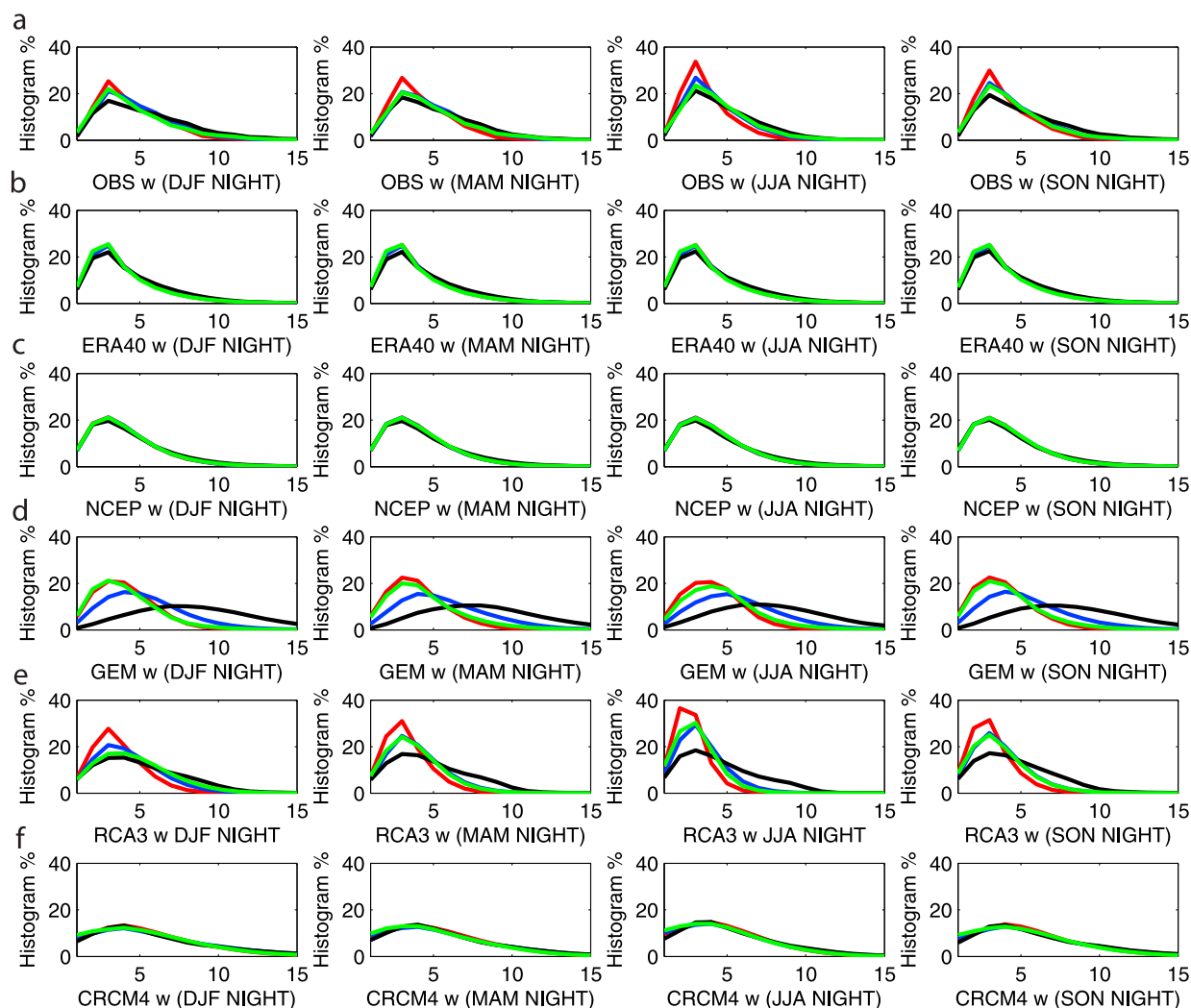


Figure 8. Comparisons of nighttime North American domain $NAP(w)$ histogram (%) over mountain (green), forest (red), open land (blue), and open water (black) from (a) observations, (b) ERA-40, (c) NCEP NCAR, (d) RCA3, (e) GEM-LAM, and (f) CRCM4 in four seasons during 1979–1999.

surface type before being grid-averaged. In forest-dominated regions it may be more appropriate to compare observed surface wind speeds with those from the open-land fraction of the same forest-dominated grid box. It is found (not shown) that over forest-dominated regions the RCA3 grid box-averaged wind speed has very few occurrences of $w > 6$ m/s while the $NAP(w)$ for the RCA3 open-land fraction wind from the same forest-dominated grid boxes is closer to that of observations, with a longer tail extending to wind speed occurrences greater than 6 m/s. This result reinforces the care that must be taken in comparing grid box-averaged quantities directly with station observations in regions of strong surface heterogeneity.

[27] The sensitivity of RCM simulations to their lateral boundary conditions (LBC) is also tested based on two GEM-LAM runs using ERA-40 reanalysis and NCEP NCAR reanalysis during the period from January 1998 to December 1999 (not shown). It is found that GEM-LAM $NAP(w)$ shows a small day-night difference over forest and no day-night difference over open water-dominated regions in both LBC runs. The details of the boundary conditions

also have little impact on the sensitivity of $NAP(w)$ to the underlying surface such as forest and open-water regions.

4. A Simple Stochastic Model Study on Surface Buoyancy Effects on Nighttime SWS PDF

[28] Monahan [2004, 2006a] used an idealized model of the boundary layer momentum budget to demonstrate the influence of surface drag on the ocean surface wind PDF under conditions of neutral stratification and constant boundary layer height. Over land, the surface buoyancy flux plays an important role in the near surface momentum budget through its effect on both drag at surface and entrainment at the boundary layer top. In this study, we particularly interested in how the dependence of the surface drag coefficient on surface buoyancy flux variations affects land SWS PDF at night. As illustrated in previous sections, the daytime SWS PDF collapses well onto the Weibull distribution over four land surface types in all seasons; at night, however, the SWS PDF shows a much broader range of skewness values well above those of a Weibull distributed quantity. This section will generalize the stochastic

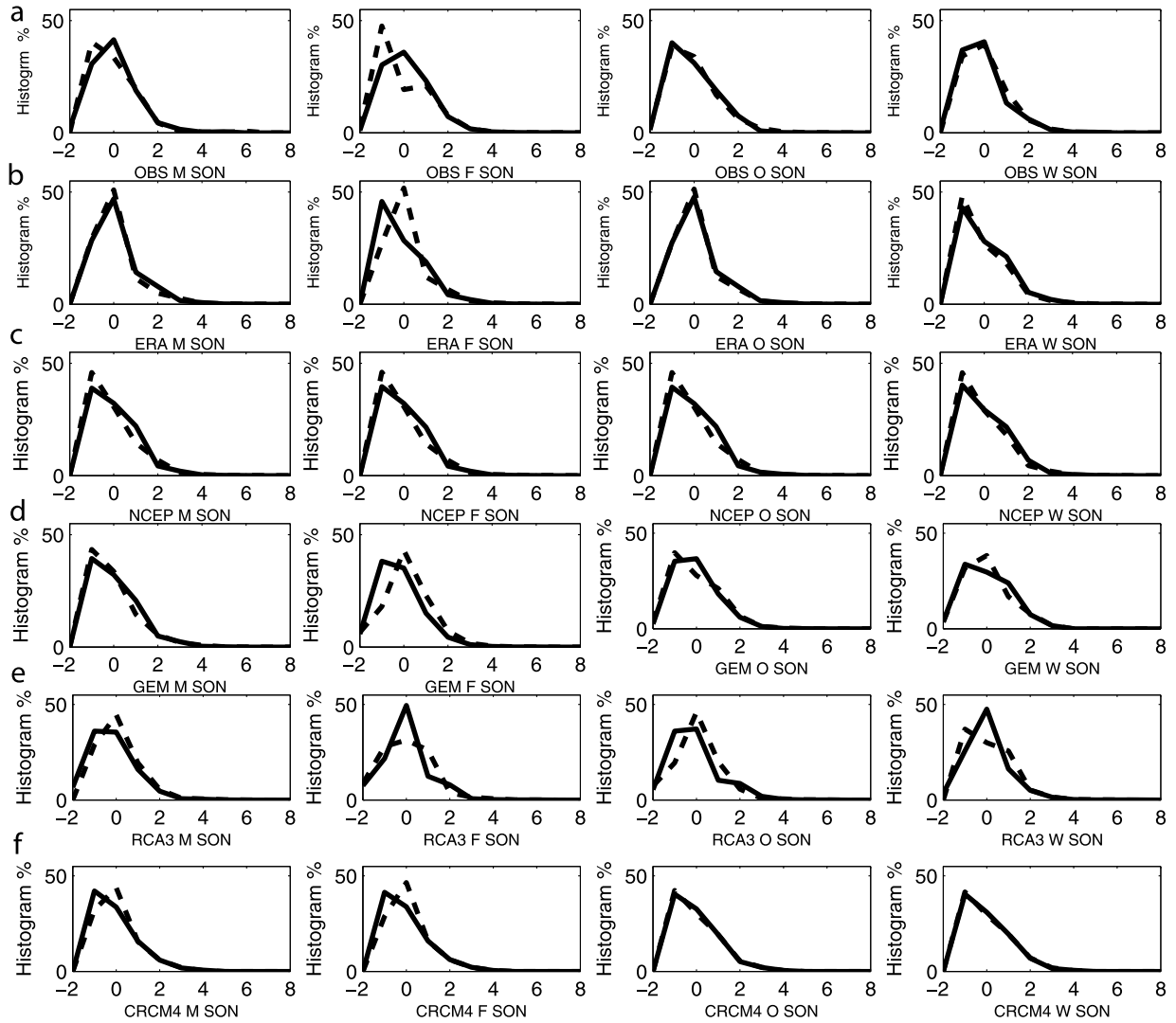


Figure 9. Comparisons of standardized daytime (solid line) and nighttime (dashed line) SON North American domain $NAP(w')$ histogram (%) among results from (a) observations, (b) ERA-40, (c) NCEP NCAR, (d) RCA3, (e) GEM-LAM, and (f) CRCM4 over (left to right) mountain (M), forest (F), open land (O), and open water (W) during 1979–1999.

model of *Monahan* [2004, 2006a] to investigate if the stable stratification of the nocturnal boundary layer can account for the non-Weibull behavior of nighttime SWS PDF. The answer to this question can improve our understanding of physical controls on the SWS PDF and give directions for future improvements of reanalysis and RCM simulations over North America.

[29] Following *Monahan* [2006a], we consider a “single-column” momentum budget (neglecting horizontal advection) and model the boundary layer momentum tendency as resulting from an imbalance between surface drag, downward mixing of momentum, and mean ($\langle F_u \rangle$ and $\langle F_v \rangle$) and fluctuating ($\Sigma \dot{W}_i$) components of the net “large-scale” forcing,

$$\dot{u} = \langle F_u \rangle - \frac{C_d(w, F)}{h} wu - \frac{K}{h^2} u + \Sigma \dot{W}_1 \quad (1)$$

$$\dot{v} = \langle F_v \rangle - \frac{C_d(w, F)}{h} wv - \frac{K}{h^2} v + \Sigma \dot{W}_2. \quad (2)$$

Here u and v are the zonal and meridional wind components; $\langle F_u \rangle$ and $\langle F_v \rangle$ represent contributions from the mean ageostrophic forces (defined as the difference between pressure gradient and Coriolis forces) and free atmosphere winds [see also *Monahan*, 2006a, equation (21)]; K is a kinematic eddy viscosity; h is the boundary layer height; \dot{W} are white noise processes; and Σ tunes the strength of fluctuations. For the stochastic model as formulated here it makes sense to write K/h^2 as w_e/h , where w_e is the entrainment velocity at the top of the boundary layer of thickness h . Based on classical Monin-Obukhov theory [*Garratt*, 1992], the surface drag coefficient C_d is given by

$$C_d = k^2 / [\ln(z/Z_0) - \Psi_M(\zeta(F_b))]^2. \quad (3)$$

Here Z_0 is the surface roughness length and Ψ_M is an empirical stability function that depends on surface buoyancy flux F_b through the Obukhov length $\zeta(F_b)$. The surface buoyancy flux (with units of $W m^{-2}$) can be calculated from

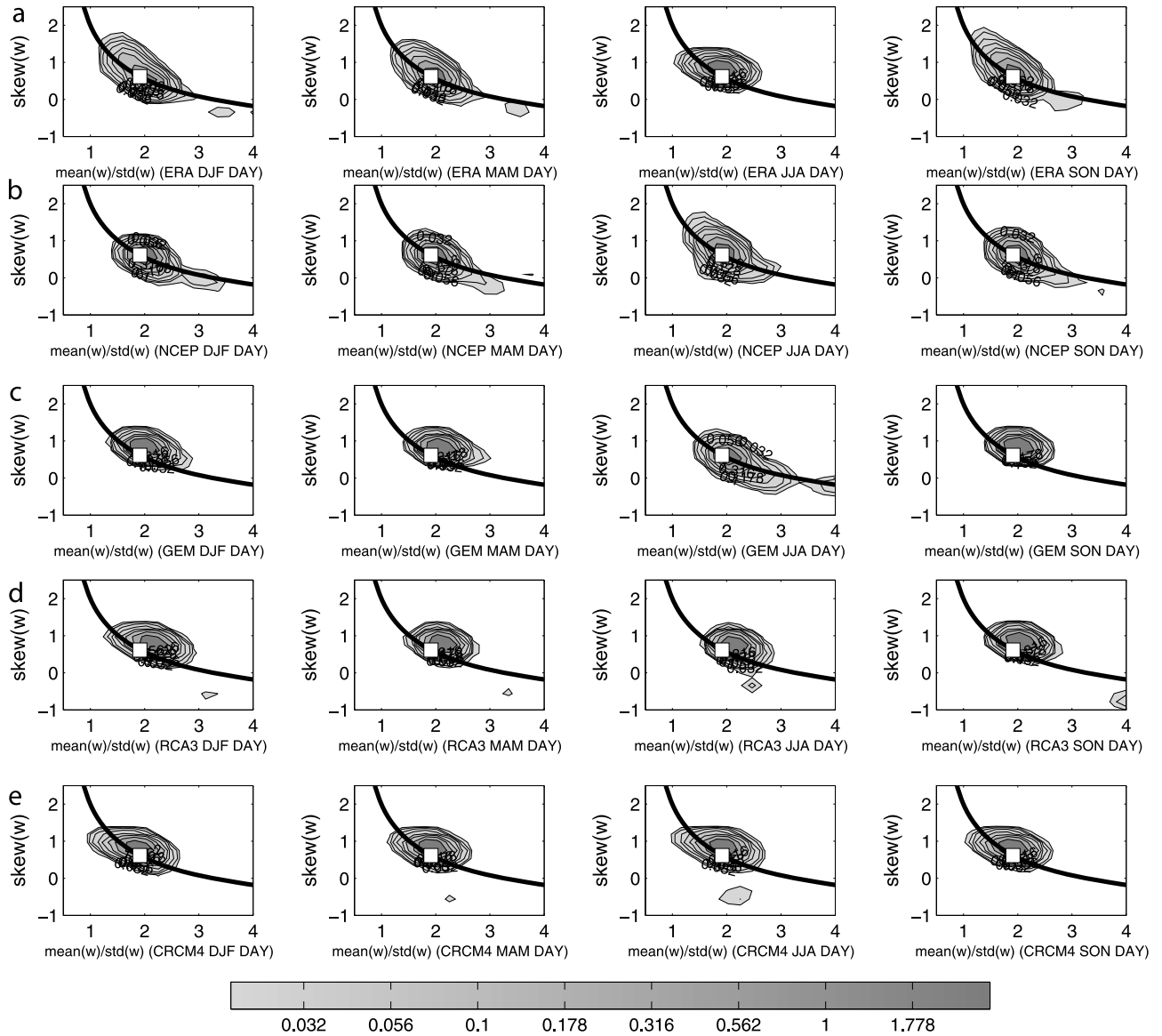


Figure 10. Kernel density estimates of joint pdfs of $\text{mean}(w)/\text{std}(w)$ and $\text{skew}(w)$ for (a) ERA-40 reanalysis, (b) NCEP NCAR reanalysis, (c) RCA3, (d) GEM-LAM, and (e) CRCM4 regional climate models in daytime four seasons during 1979–1999. The contour intervals are logarithmically spaced. The solid line is the theoretical curve for a Weibull variable, and the white square corresponds to a Rayleigh variable.

surface sensible heat flux F_{SH} and surface latent heat flux F_{LH} assuming constant potential temperature θ_0 [Garratt 1992],

$$F_b = F_{SH} + 0.61 \times \theta_0 \times \frac{C_p}{L_v} F_{LH}. \quad (4)$$

In neutral conditions, Ψ_M is zero so C_d is a function of surface roughness Z_0 alone (this is the case considered by Monahan [2004, 2006a]). The surface drag coefficient C_d increases for larger surface roughness Z_0 . In unstable conditions ($\zeta < 0$), $\Psi_M > 0$; and the drag coefficient is larger than in the neutral case; in stable conditions ($\zeta > 0$), $\Psi_M < 0$ and the drag coefficient is smaller than in the neutral

case. Following Miyakoda and Sirutis [1986], the empirical functional form of the Monin-Obukhov similarity function Ψ_M from Businger *et al.* [1971] and Hicks [1976] is used in these calculations [cf. Miyakoda and Sirutis, 1986]. It is implicitly assumed in this stochastic model that the surface buoyancy fluxes evolve on time scales longer than those of the surface winds, and that the fluxes can be specified independent of surface wind speeds. The consequences of these assumptions will be discussed in section 5.

[30] Figure 12 illustrates the dependence of the drag coefficient C_d on both w and surface buoyancy flux F_b from model simulations, in which the reference height is set to 10 m, the surface roughness $Z_0 = 0.1$ m, and the reference temperature is $\theta_0 = 290$ K. It is evident that C_d decreases with w for $F_b > 0$ but increases with w for $F_b < 0$. In a

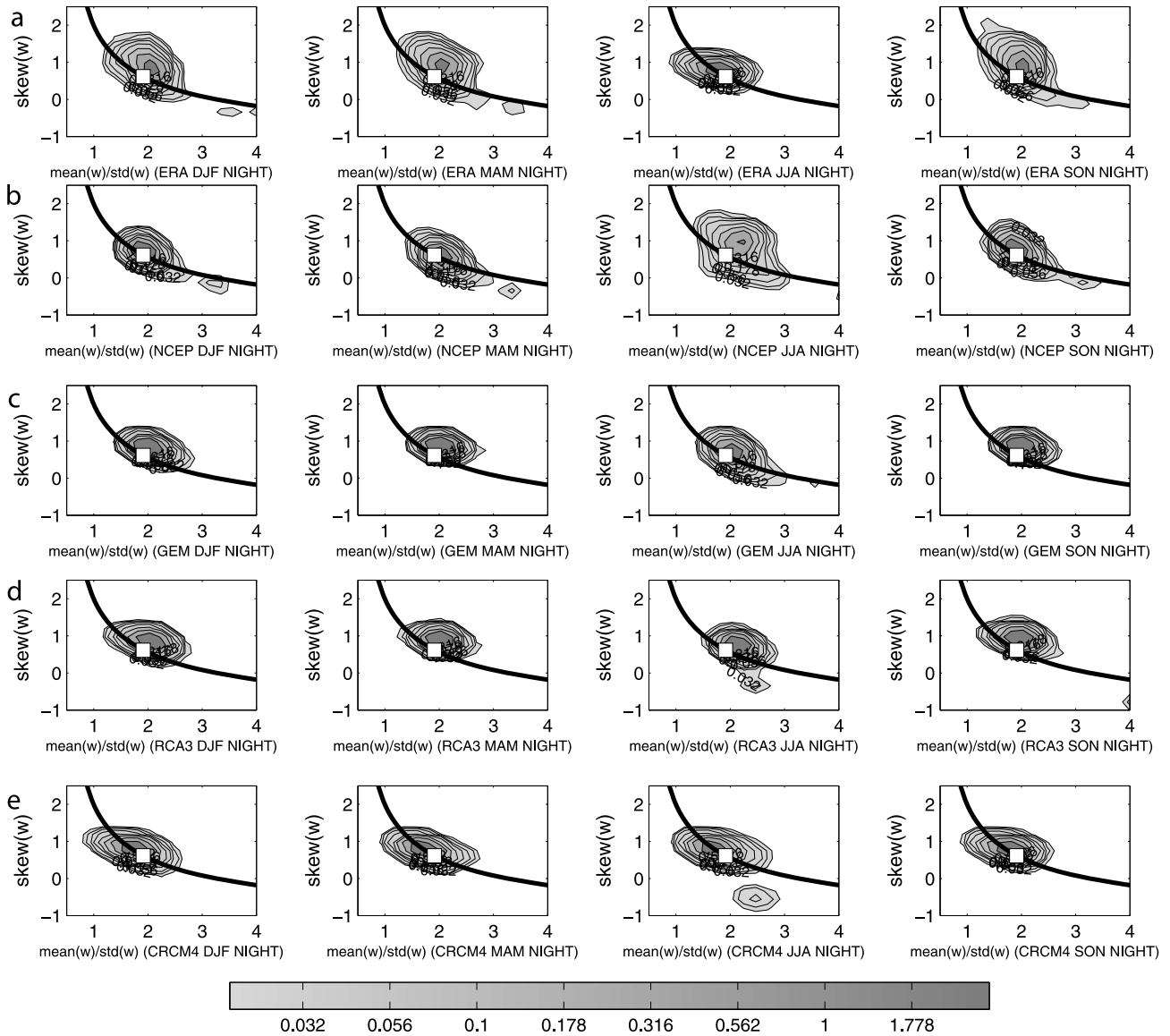


Figure 11. As in Figure 10 but for the nighttime case.

neutral boundary layer with zero buoyancy flux, C_d is independent of SWS; while in regimes of small w and a very stable surface layer, C_d approaches zero. The drag coefficient C_d is an increasing function of F_b in both stable and unstable surface layers.

[31] The SWS PDF (here denoted $p(w)$) is formulated as following:

$$p(w) = \int p(w|F_b)p(F_b)dF_b, \quad (5)$$

where $p(w|F_b)$ is the conditional probability distribution of w given F_b . For simplicity, the surface buoyancy flux F_b is treated as an external Gaussian random variable.

$$p(F_b) = \frac{1}{\sqrt{2\pi}\sigma_{F_b}} \exp\left(-\frac{(x - \mu_{F_b})^2}{2\sigma_{F_b}^2}\right). \quad (6)$$

Here μ_{F_b} and σ_{F_b} are the specified mean and standard deviation of F_b , respectively. Assuming that F_b evolves over longer time scales than w , we can compute $p(w|F_b)$ using the analytical formulation of the probability distribution of SWS for a given (wind speed dependent) drag coefficient from *Monahan* [2006a].

$$p(w|F_b) = G(w) \exp\left[\left(-\frac{2}{\Sigma^2 h} \int_0^w C_d(F_b, w')w'^2 dw'\right)\right] \quad (7)$$

$$G(w) = N_1 w I_0 \frac{2 \langle F_u \rangle w}{\Sigma^2} \exp\left(-\frac{K^2}{\Sigma^2 h^2} w^2\right). \quad (8)$$

Here I_0 is the modified Bessel function of order zero. Figure 13 displays the simulated SWS moments (mean(w), std(w), skew(w)) and the normalized mean wind speed mean(w)/std(w) as a function of mean(F_b) and std(F_b) for fixed external forcing and surface roughness. Both mean(w)

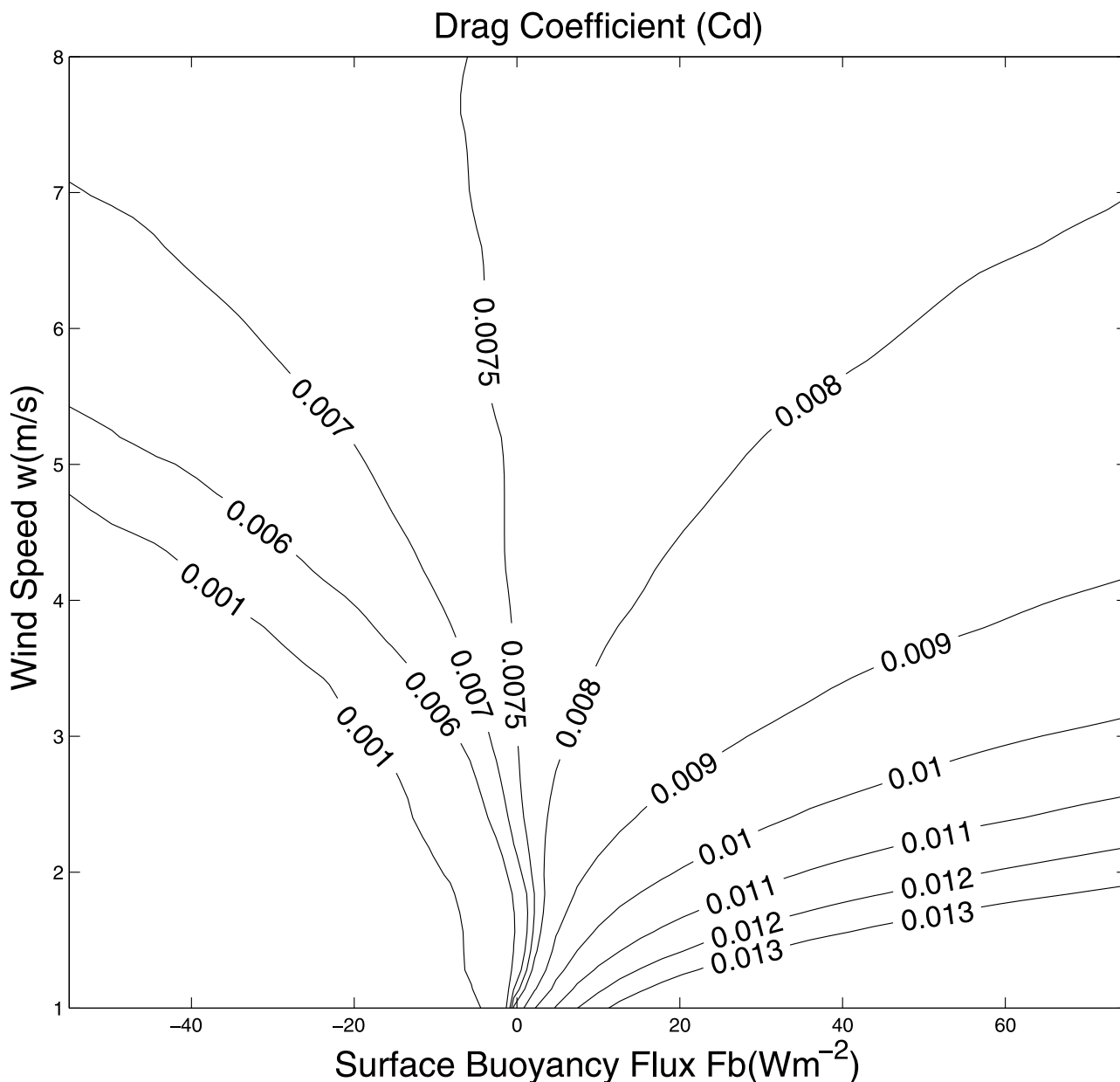


Figure 12. Variations of drag coefficient C_d as an empirical function of 10 m wind speed w (m/s) and surface buoyancy flux (W m^{-2}). The stability dependence form is determined empirically after *Businger et al.* [1971] and *Hicks* [1976]. The reference height is set to 10 m, the surface roughness $Z_0 = 0.1$ m, and the reference potential temperature $\theta_0 = 290$ K.

and $\text{std}(w)$ show negative relationships with $\text{mean}(F_b)$. In contrast, the wind speed skew(w) has a positive relationship with both $\text{mean}(F_b)$ and $\text{std}(F_b)$. The stochastic model-simulated relationship between SWS moments and surface buoyancy flux is consistent with the observed nighttime relationships illustrated in Figure 14, which shows the relationship between the observed SWS moments and the mean RCA3 surface buoyancy flux F_b (calculated from 3-hourly surface sensible and latent heat fluxes from RCA3 fields at grid points nearest the station locations using equation (4) and assuming $\rho_0 = 290$ K) over mountain- and open land-dominated regions in the seasons of JJA and SON. It is worth noting that no simple observed relationship

is found over open water-dominated regions where both surface friction and surface buoyancy flux are small. It is also difficult to match RCM simulated surface buoyancy to the observed SWS in forest areas because weather station wind is measured at approximately 10 m in an open area near or within forest sites while surface buoyancy flux is simulated above the canopy (with canopy height as high as 30 m or above) over forest regions in RCMs.

[32] An important feature shown in Figure 13 is that the change rate of skew(w) with increasing $\text{mean}(F_b)$ is substantially greater in the stable PBL (negative $\text{mean}(F_b)$) than that in the unstable PBL (positive $\text{mean}(F_b)$); while the normalized wind speed varies over a small range. This

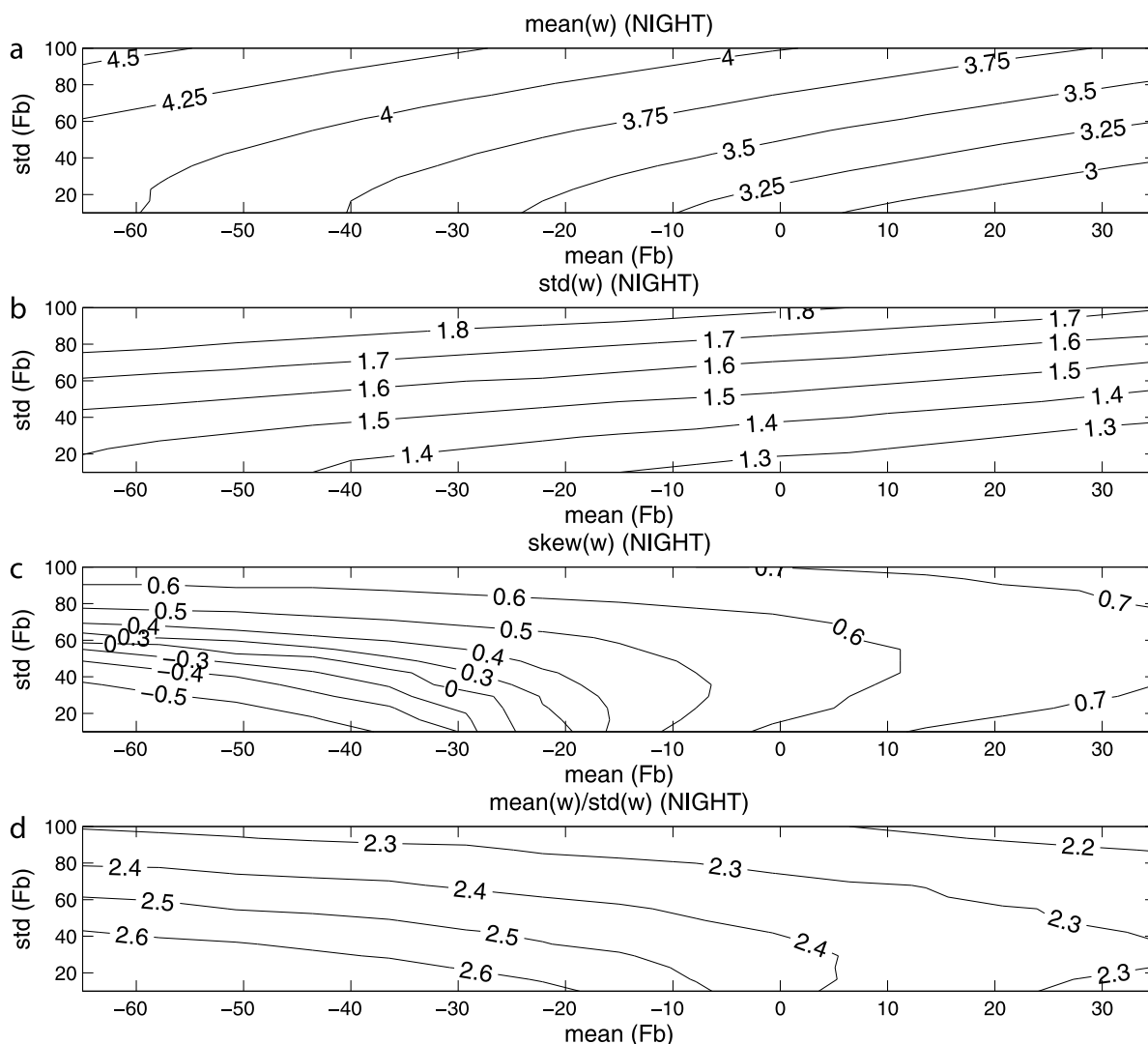


Figure 13. Simulated (a) $\text{mean}(w)$, (b) $\text{std}(w)$, (c) $\text{skew}(w)$, and (d) $\text{mean}(w)/\text{std}(w)$ as a function of both mean and standard deviation of buoyancy flux in the idealized, stochastic model described in section 4 (with parameter values: $\langle F_u \rangle = 6 \times 10^{-5} \text{ m s}^{-2}$, $\Sigma^2 = 0.001 \text{ m s}^{-3/2}$, $K = 1.0$, $h = 300 \text{ m}$, and $Z_0 = 0.1 \text{ m}$).

stochastic model result is consistent with land surface observations shown in Figures 4 and 6, in which the SWS PDF at night (stable stratification on average) has a much broader range of skewness near and above the Weibull distribution than that in the day (unstable stratification on average). Furthermore, a preliminary analysis of the RCA3 surface flux climatology (not shown) indicates that strongly negative mean surface fluxes are associated with strong surface flux variability. Inspection of Figure 13c indicates that this fact is consistent with the observed nighttime large positive skewnesses. It is worth noting that the relationship between the leading three moments of observed SWS and surface buoyancy flux as illustrated in Figure 14 is also characteristic of fluxes taken from the NCEP-NCAR reanalysis (not shown here).

[33] These results illustrate that surface buoyancy fluxes modulate the SWS PDF (both in magnitudes of values and PDF shape) in a manner that can be accounted for by an idealized model of the boundary layer momentum budget. A

more thorough investigation of the influence of surface buoyancy fluxes on the SWS PDF will be investigated in a future study.

5. Summary and Conclusions

[34] Knowledge of the land surface wind PDF is important for many applications in surface flux estimation, wind resource assessment, and extreme weather forecasting. The two-parameter Weibull distribution is the most widely used empirical model of the SWS PDF. In this study we have considered seasonal, diurnal, and land surface type influences on the observed SWS PDF to identify those circumstances in which the Weibull distribution is a good fit to observed variability and to identify influences of surface buoyancy fluxes on the PDF. A comparison of observed SWS PDF with that simulated in two reanalysis products and three regional climate model (RCMs) simulations was done to determine the ability of these models to represent

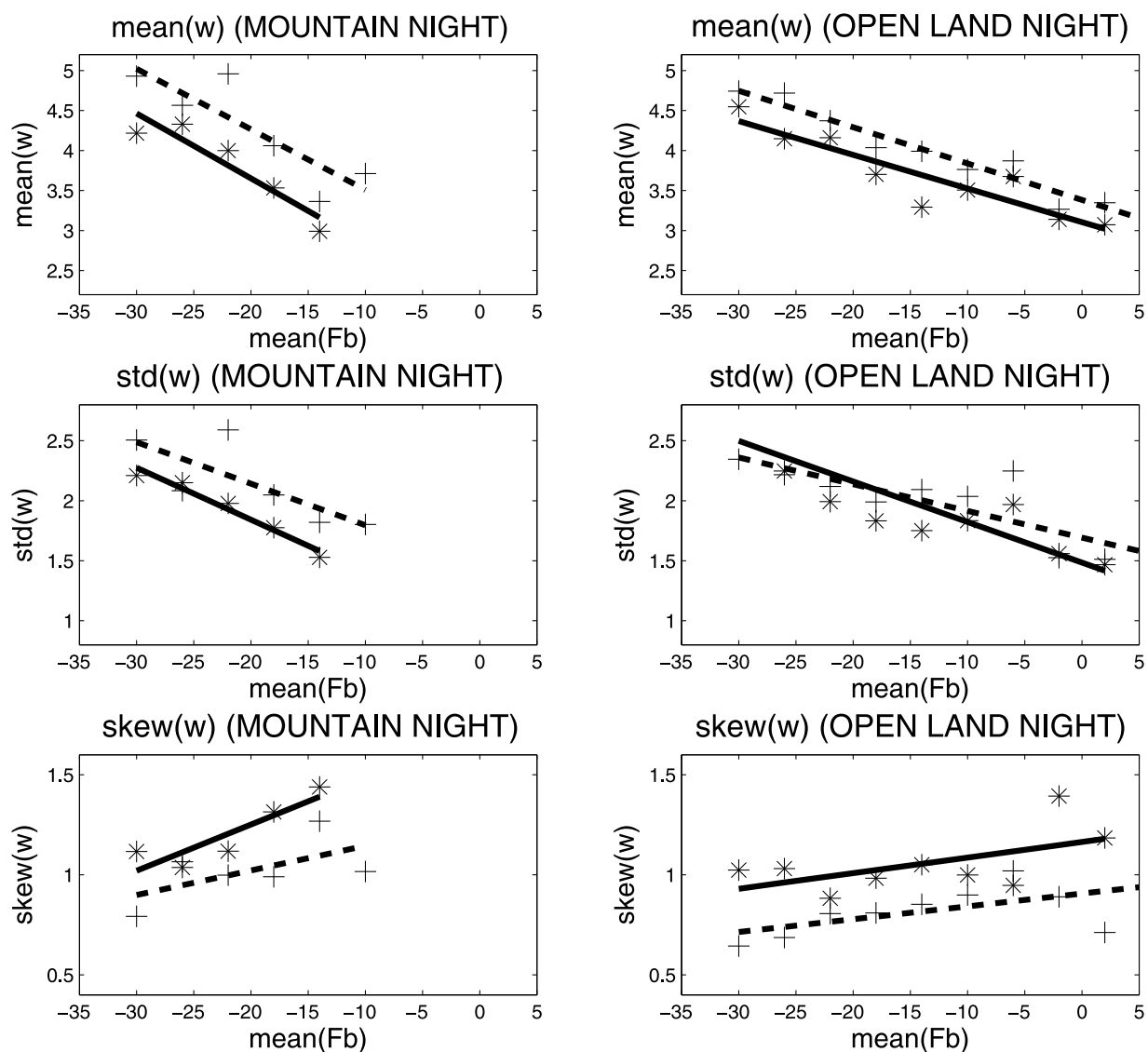


Figure 14. The nighttime (top) $\text{mean}(w)$, (middle) $\text{std}(w)$, and (bottom) $\text{skew}(w)$ as a function of the RCA3 mean surface buoyancy flux over (left) mountain-dominated regions and (right) open land-dominated regions in JJA (stars) and SON (pluses) seasons during 1979–1999. Moments are averaged within each bin box (bin width of 5 W m^{-2}) in cases that more than three stations are available. Linear fits are also shown for JJA (solid line) and SON (dashed line).

the observed features of SWS PDF over North America. The main findings can be summarized as follows:

[35] 1. The three leading moments of SWS (characterizing both magnitudes of the winds as well as the shape of the PDF) are sensitive to the underlying land surface type, season, and phase of the diurnal cycle.

[36] 2. For daytime winds, the SWS PDF collapses well around the relationship between moments characteristic of the two-parameter Weibull distribution in all four seasons. At night, however, the observed SWS PDF over mountainous terrain, forest, and open land has a much broader range of skewness near and well above the Weibull distribution.

[37] 3. A mechanistic model study suggests that the dependence of surface drag coefficient on surface buoyancy plays a key role in diurnal variations of the SWS PDF.

Particularly noteworthy is the prediction that nighttime skewness should display greater sensitivity to both mean and standard deviation of surface buoyancy flux than daytime skewness.

[38] 4. Both reanalysis products and all three RCMs failed to simulate the strong positive values and broad range of skewness of SWS PDF at night, possibly because of problems with representing nighttime stable boundary layer turbulent mixing and/or the empirical extrapolation formula for SWS in most models and reanalysis; or their inability to represent the correct variance of surface fluxes.

[39] 5. Both the ERA-40 and NCEP NCAR reanalyses are unable to simulate the seasonal evolution and sensitivity to land surface types of the observed SWS PDF. Of the RCMs considered in this study, only the RCA is able to

capture the correct seasonality of the SWS PDF, while both the RCA and GEM-LAM capture the sensitivity to the land surface type.

[40] Accurate prediction of surface fluxes, wind energy, and wind extremes in present and future climates requires that of the PDF of surface wind speeds be represented faithfully. Current observational and empirical downscaling approaches generally assume a two-parameter Weibull distribution for the SWS PDF, taking into account variations of terrain, surface roughness, sheltering obstacles, and regional climate to make generally good predictions of the leading two SWS moments. However, this study demonstrates marked departures from Weibull behavior of nighttime SWS. In particular, nighttime SWS skewness is generally underestimated by the Weibull distribution; evidence from seasonal variability in the diurnal cycle and an idealized stochastic SWS model suggest that surface buoyancy fluxes play an important role in producing this non-Weibull behavior.

[41] It is worth noting that the surface wind probability distribution over open water shows significantly different characteristics than that over other three rough surface types. Wind speeds over open water have a Weibull like SWS PDF in both day and night and a much broader range of normalized wind speeds (consistent with the observed structure of the SWS PDF over the ocean [Monahan, 2006a, 2006b]). Surface buoyancy flux is found to play an important role over rough land surfaces; however, there is no simple relationship between surface flux and moments of surface winds over open-water regions, consistent with recent studies demonstrating that surface stratification has little direct influence (through modification of the drag coefficient) on the SWS PDF over the ocean [Capps and Zender, 2009; A. H. Monahan, The probability distribution of sea surface wind speeds: Effects of variable surface stratification and boundary layer thickness, submitted to *Journal of Climate*, 2009]. This result implies that challenges for offshore wind resource assessment may come largely from other factors such as the dependence of surface roughness on waves, stability, and water depth, and the different vertical profile of offshore winds from those found onshore [Landberg *et al.*, 2003].

[42] There are a number of potential limitations to this study that will be addressed in future work. First, some of the station wind data may contain spurious changes that could have affected the estimated PDFs. However, we believe our conclusions regarding the day-night differences and the sensitivity to land cover types and seasons are unlikely to be affected by the spurious changes. Second, as noted before, surface buoyancy affects SWS through (1) changes in surface friction; (2) downward momentum entrainment from boundary layer top; and (3) mixing layer depth variations. The current simple model (equation (1) to (6)) accounted for only the first of these. An interesting extension of the present study would be the generalization of this model to include all three effects, particularly in order to improve the model's ability to simulate both daytime and nighttime SWS PDF. Furthermore, the characterization of the relationship between surface buoyancy fluxes and the SWS PDF required use of model-based fluxes (as observational values are not directly available). The consistency of this relationship between different model

products gives us confidence that it is real and not a model artifact.

[43] Another limitation of the simple stochastic model is that the effect of SWS on surface buoyancy fluxes has not been taken into account in the present study. Instead, the surface flux is treated as a slowly varying function independent of surface wind speed (as is often done in idealized single column model studies). An interesting direction of future study would be to investigate the contribution of surface buoyancy–wind speed coupling on the SWS PDF.

[44] In summary, this work is the first attempt to characterize the SWS PDF over North America combining an analysis of extensive weather station observations with a simple stochastic model study and analyses of reanalysis and RCMs wind speed simulations. The results obtained in this study have a bearing on wind energy estimation, wind risk assessment, regional climate downscaling, and surface flux parameterization. Land surface winds are an important component of the climate system; while their sensitivity to surface heterogeneity makes them a difficult field to simulate accurately in fine detail, the results of this study indicate that the controls on their leading-order statistical features may in fact be amenable to elementary physical understanding.

Appendix A: Sensitivity of Leading Moments of Surface Wind Speed to the Most Extreme Observations

[45] The top 0.5% of wind records from weather stations was removed before calculating the leading moments and regional probability distributions of the surface wind speed. The main reason for this data preprocessing was that in this study we focus on the probability distribution of routine surface winds, rather than the most extreme events. The former are responsible for the bulk of wind energy production [Petersen *et al.*, 1998a, 1998b] and also play an important role in surface flux parameterizations in climate models. Another reason is that observational errors may disproportionately influence higher-order statistical moments. In some cases, there are reports of extreme weather phenomena or related surface variable changes within a few hours of the reported extreme wind event. However, in other cases, there are no reports of abnormal weather phenomena or related surface variable changes near the extreme wind event indicating the presence of human or instrumental errors associated with some of the extreme wind records. The focus of this study is the probability distribution of “routine” surface winds of most relevance to wind power generation and surface fluxes, so these most extreme wind records were excluded from the computations. To assess the sensitivity of the results of this study to the fraction of extreme wind data excluded, the analyses were repeated excluding different percentages of extreme data.

[46] The leading moments (averaged over North America) of surface wind speed calculated by removing the top 0.25%, 0.5%, and 0.75% of wind records show all three moments are reduced when more extreme winds are excluded from the calculation. In most cases, the domain-averaged mean and the standard deviation are reduced only slightly (by less than 0.05 m/s and 0.1 m/s, respectively) between the case in which the top 0.75% of observations are

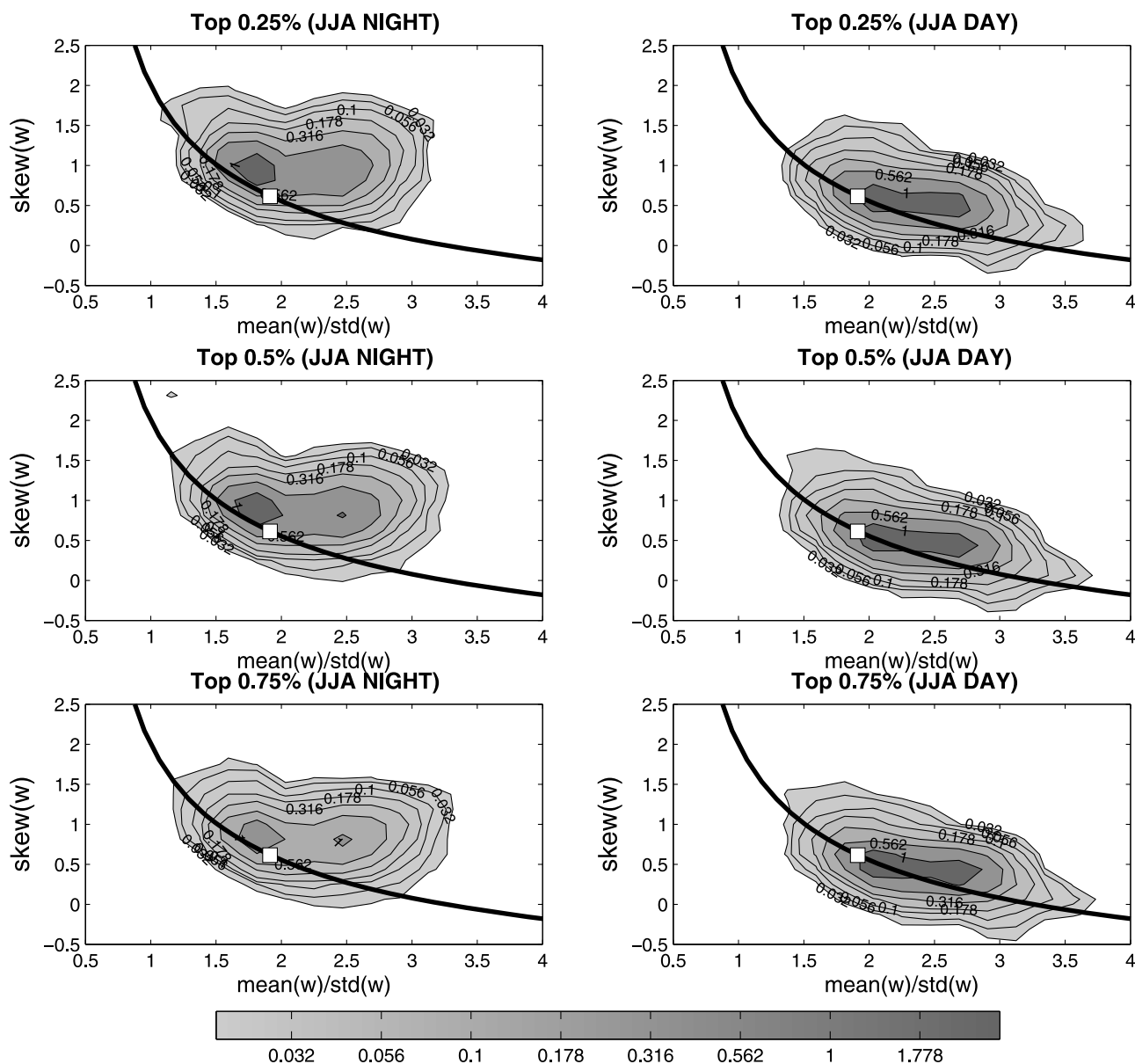


Figure A1. Kernel density estimates of joint pdfs of $\text{mean}(w)/\text{std}(w)$ and $\text{skew}(w)$ for observations over all surface types in three cases (removing top 0.25%, removing top 0.5%, and removing top 0.75%) in (right) day and (left) night in JJA during the study period. The contour intervals are logarithmically spaced. The solid line is the theoretical curve for a Weibull variable; the white square corresponds to a Rayleigh variable.

excluded and the case in which 0.25% are excluded. However, the averaged skewness is reduced by as much as 0.2 in some cases.

[47] Figure A1 shows the observed DJF relationship between grid point wind speed skewness and normalized wind speed over forest-dominated land surface calculated by removing the top 0.25%, 0.5%, and 0.75% of the wind records. It is evident that while the values of individual moments display some sensitivity to the exclusion of extreme data, the relationship between moments is not sensitive. Changing the fraction of data excluded from the analysis over the range considered does not alter the character of the surface wind speed PDFs.

[48] **Acknowledgments.** This research is supported by Mathematics and Information Technology of Complex System (MITACS) project supported by Simon Fraser University and Ouranos and the Canadian Regional Climate Modeling and Diagnosis (CRCMD) network supported by CFCAS and Ouranos. Adam Monahan also acknowledges support from the Canadian Institute for Advanced Research Earth Systems Evolution Program. We also thank AmeriFlux network for providing continuous observations of wind speed data above canopy at various forest sites. We thank three anonymous reviewers for greatly improving the quality of this paper.

References

- Archer, C. L., and M. Z. Jacobson (2003), Spatial and temporal distribution of U.S. winds and wind power at 80 m derived from measurements, *J. Geophys. Res.*, *108*(D9), 4289, doi:10.1029/2002JD002076.
- Archer, C. L., and M. Z. Jacobson (2005), Evaluation of global wind power, *J. Geophys. Res.*, *110*, D12110, doi:10.1029/2004JD005462.

- Businger, J. A., J. C. Wyngaard, Y. Izumi, and E. F. Bradley (1971), Flux-profile relationships in the atmospheric surface layer, *J. Atmos. Sci.*, **28**, 181–189, doi:10.1175/1520-0469(1971)028<0181:FPRTA>2.0.CO;2.
- Capps, S. B., and C. S. Zender (2009), Global ocean wind power sensitivity to surface layer stability, *Geophys. Res. Lett.*, **36**, L09801, doi:10.1029/2008GL037063.
- Caya, D., and R. Laprise (1999), A semi-implicit semi-Lagrangian regional climate model: The Canadian RCM, *Mon. Weather Rev.*, **127**, 341–362, doi:10.1175/1520-0493(1999)127<0341:ASISLR>2.0.CO;2.
- Conradsen, K., and L. B. Nielsen (1984), Review of Weibull statistics for estimation of wind speed distributions, *J. Appl. Meteorol.*, **23**, 1173–1183, doi:10.1175/1520-0450(1984)023<1173:ROWSFE>2.0.CO;2.
- Cote, J., S. Gravel, A. Methot, A. Patoine, M. Roch, and A. Staniforth (1998), The operational CMC-MRB Global Environmental Multiscale (GEM) model. Part I: Design considerations and formulation, *Mon. Weather Rev.*, **126**, 1373–1395, doi:10.1175/1520-0493(1998)126<1373:TOCMGE>2.0.CO;2.
- Dai, A., and C. Deser (1999), Diurnal and semidiurnal variations in global surface wind and divergence fields, *J. Geophys. Res.*, **104**(D24), 31,109–31,125, doi:10.1029/1999JD900927.
- Dai, A., T. R. Karl, B. Sun, and K. E. Trenberth (2006), Recent trends in cloudiness over the United States: A tale of monitoring inadequacies, *Bull. Am. Meteorol. Soc.*, **87**, 597–606, doi:10.1175/BAMS-87-5-597.
- De Elia, R., D. Caya, H. Cote, A. Frigon, S. Biner, M. Giguere, D. Paquin, R. Harvey, and D. Plummer (2007), Evaluation of uncertainties in the CRCM-simulated North American climate, *Clim. Dyn.*, **30**, 113–132, doi:10.1007/s00382-007-0288-z.
- Doesken, N. J., T. B. McKee, and C. Davey (2002), Climate data continuity: What have we learned from the AUTOMATED surface Observing System (ASOS), paper presented at 13th AMS Conference on Applied Climatology, Am. Meteorol. Soc., Portland, Oreg.
- Elliott, D. L., C. G. Holladay, W. R. Barchet, H. P. Foote, and W. F. Sandusky (1986), Wind energy resource atlas of the United States, *DOE/CH 10093-4*, Natl. Renewable Energy Lab., Golden, Colo.
- Frey-Buness, F., D. Heimann, and R. Sausen (1995), A statistical-dynamical downscaling procedure for global climate simulations, *Theor. Appl. Climatol.*, **50**, 117–131, doi:10.1007/BF00866111.
- Garratt, J. R. (1992), *The Atmospheric Boundary Layer*, Cambridge Univ. Press, Cambridge, U. K.
- Hennessey, J. P., Jr. (1977), Some aspects of wind power statistics, *J. Appl. Meteorol.*, **16**, 119–128, doi:10.1175/1520-0450(1977)016<0119:SAOWPS>2.0.CO;2.
- Hicks, B. B. (1976), Wind profile relationships from “Wangara” experiments, *Q. J. R. Meteorol. Soc.*, **102**, 535–551.
- Jagger, T., J. B. Elsner, and X. Niu (2001), A Dynamic probability model of hurricane winds in coastal counties of the United States, *J. Appl. Meteorol.*, **40**, 853–863, doi:10.1175/1520-0450(2001)040<0853:ADPMOH>2.0.CO;2.
- Jones, C. G., U. Willén, A. Ullerstig, and U. Hanssons (2004), The Rossby Centre Regional Atmospheric Climate Model Part I: Model climatology and performance for the present climate over Europe, *Ambio*, **33**(4–5), 199–210.
- Justus, C. G., W. R. Hargraves, and A. Yalcin (1976), Nationwide assessment of potential output from wind-powered generators, *J. Appl. Meteorol.*, **15**, 673–678, doi:10.1175/1520-0450(1976)015<0673:NAOPOF>2.0.CO;2.
- Justus, C. G., W. R. Hargraves, A. Mikhail, and D. Graber (1978), Methods for estimating wind speed frequency distributions, *J. Appl. Meteorol.*, **17**, 350–353, doi:10.1175/1520-0450(1978)017<0350:MFEWSF>2.0.CO;2.
- Kalnay, E., et al. (1996), The NCEP-NCAR 40-year reanalysis project, *Bull. Am. Meteorol. Soc.*, **77**, 437–471, doi:10.1175/1520-0477(1996)077<0437:TNYRP>2.0.CO;2.
- Kjellström, E., L. Bärring, S. Gollvik, U. Hansson, C. Jones, P. Samuelsson, M. Rummukainen, A. Ullerstig, U. Willén, and K. Wyser (2005), A 140-year simulation of European climate with the new version of the Rossby Centre regional atmospheric climate model (RCA3), *Rep. Meteorol. Climatol.*, **108**, 54 pp., SMHI, Norrköping, Sweden.
- Landberg, L., L. Myllerup, O. Rathmann, E. L. Petersen, B. H. Jørgensen, J. Badger, and N. G. Mortensen (2003), Wind resource estimation—An overview, *Wind Energy*, **6**, 261–271, doi:10.1002/we.94.
- Linacre, E. (1992), *Climate Data and Resources: A Reference and Guide*, 366 pp., Routledge, Boca Raton, Fla.
- Masson, V., C. Jean-Louis, C. Fabrice, M. Christelle, and L. Roselyne (2003), A global database of land surface parameters at 1-km resolution in meteorological and climate models, *J. Clim.*, **16**, 1261–1282.
- Meeus, J. (1998), *Astronomical Algorithms*, 2nd ed., Willmann-Bell, Richmond, Va.
- Miyakoda, K., and J. Sirutis (1986), *Manual of E-Physics: The GFDL Report*, Geophys. Fluid Dyn. Lab., NOAA, Silver Spring, Md.
- Monahan, A. H. (2004), A simple model for the skewness of global sea-surface winds, *J. Atmos. Sci.*, **61**, 2037–2049, doi:10.1175/1520-0469(2004)061<2037:ASMFTS>2.0.CO;2.
- Monahan, A. H. (2006a), The probability distribution of sea surface wind speeds. Part I: Theory and sea winds observations, *J. Clim.*, **19**, 497–520, doi:10.1175/JCLI3640.1.
- Monahan, A. H. (2006b), The probability distribution of sea surface wind speeds. Part II: Dataset intercomparison and seasonal variability, *J. Clim.*, **19**, 521–534, doi:10.1175/JCLI3641.1.
- Mortensen, N. G., L. Landberg, I. Troen, and E. L. Petersen (1993), Wind Atlas Analysis and Application Program (WAsP). Vol. 1: Getting started, *Risø-I-666(EN)*, Risø Natl. Lab., Roskilde, Denmark.
- National Weather Service (1992), ASOS (Automated Surface Observing System) user’s guide, report, 57 pp., NOAA, Silver Spring, Md.
- Pavia, E. G., and J. J. O’Brien (1986), Weibull statistics of wind speed over the Ocean, *J. Clim. Appl. Meteorol.*, **25**, 1324–1332, doi:10.1175/1520-0450(1986)025<1324:WSOWSO>2.0.CO;2.
- Petersen, E. L., N. G. Mortensen, L. Landberg, J. Hojstrup, and H. P. Frank (1998a), Wind power meteorology Part I: Climate and turbulence, *Wind Energy*, **1**, 25–45, doi:10.1002/(SICI)1099-1824(199804)1:1<25::AID-WE4>3.3.CO;2-4.
- Petersen, E. L., N. G. Mortensen, L. Landberg, J. Hojstrup, and H. P. Frank (1998b), Wind power meteorology Part II: Siting and models, *Wind Energy*, **1**, 55–72, doi:10.1002/(SICI)1099-1824(199812)1:2<55::AID-WE5>3.0.CO;2-R.
- Plummer, D. A., D. Caya, A. Frigon, H. Cote, M. Giguere, D. Paquin, S. Biner, R. Harvey, and R. De Elia (2006), Climate and climate change over North America as simulated by the Canadian RCM, *J. Clim.*, **19**, 3112–3132, doi:10.1175/JCLI3769.1.
- Pryor, S. C., R. J. Barthelmie, and E. Kjellstrom (2005a), Potential climate change impact on wind energy resources in northern Europe: Analyses using a regional climate model, *Clim. Dyn.*, **25**, 815–835, doi:10.1007/s00382-005-0072-x.
- Pryor, S. C., J. T. Schoof, and R. J. Barthelmie (2005b), Empirical downscaling of wind speed probability distributions, *J. Geophys. Res.*, **110**, D19109, doi:10.1029/2005JD005899.
- Quine, C. P. (2000), Estimation of mean wind climate and probability of strong winds for wind risk assessment, *Forestry*, **73**(3), 248–258.
- Rockel, B., and K. Woth (2007), Extremes of near-surface wind speed over Europe and their future changes as estimated from an ensemble of RCM simulations, *Clim. Change*, **81**, 267–280, doi:10.1007/s10584-006-9227-y.
- Segal, M., Z. Pan, R. W. Arritt, and E. S. Takle (2001), On the potential change in wind power over the US due to increases of atmospheric greenhouse gases, *Renewable Energy*, **24**, 235–243, doi:10.1016/S0960-1481(00)00194-4.
- Stewart, D. A., and O. M. Essenwanger (1978), Frequency distribution of wind speed near the surface, *J. Appl. Meteorol.*, **17**, 1633–1642, doi:10.1175/1520-0450(1978)017<1633:FDOWSN>2.0.CO;2.
- Sura, P., M. Newman, and M. A. Alexander (2006), Daily to decadal sea surface temperature variability driven by state-dependent stochastic heat fluxes, *J. Phys. Oceanogr.*, **36**, 1940–1958, doi:10.1175/JPO2948.1.
- Tuller, S., and A. C. Brett (1984), The characteristics of wind velocity that favor the fitting of a Weibull distribution in wind speed analysis, *J. Clim. Appl. Meteorol.*, **23**, 124–134, doi:10.1175/1520-0450(1984)023<0124:TCOWVT>2.0.CO;2.
- Uppala, S. M., et al. (2005), The ERA-40 re-analysis, *Q. J. R. Meteorol. Soc.*, **131**, 2961–3012, doi:10.1256/qj.04.176.
- Zadra, A., D. Caya, J. Côté, B. Dugas, C. Jones, R. Laprise, K. Winger, and L. P. Caron (2008), The next Canadian Regional Climate Model, in press, *Phys. Can.*, **64**, 75–83.

S. Biner and D. Caya, Ouranos, Montreal, QC H3A 1B9, Canada.

A. Dai, National Center for Atmospheric Research, Boulder, CO 80307, USA.

Y. He and A. H. Monahan, School of Earth and Ocean Science, University of Victoria, Victoria, BC V8W 3P6, Canada. (yhe@uvic.ca)

C. G. Jones and K. Winger, Centre ESCER, University of Quebec at Montreal, Montreal, QC H3C 3P8, Canada.